Humoral immunity to SARS-CoV-2 elicited by combination COVID-19 vaccination regimens

Zijun Wang [1,*], Frauke Muecksch[2,*], Friederike Muenn [3,*], Alice Cho[1,*], Shuai Zong[1], Raphael Raspe[1], Victor Ramos[1], Brianna Johnson[1], Tarek Ben Tanfous[1], Justin DaSilva[2], Eva Bednarski[2], Camila Guzman-Cardozo[2], Martina Turroja[1], Katrina G. Millard[1], Pinkus Tober-Lau[3], David Hillus[3], Kai-Hui Yao[1], Irina Shimeliovich[1], Juan Dizon[1], Anna Kaczynska[1], Mila Jankovic[1], Anna Gazumyan[1], Thiago Y. Oliveira[1], Marina Caskey[1], Paul D. Bieniasz[2,4], Theodora Hatziioannou[2], Florian Kurth[3], Leif Erik Sander[3,5], Michel C. Nussenzweig[1,4,#] and Christian Gaebler[1,3,#]

[1]Laboratory of Molecular Immunology, The Rockefeller University, New York, NY, USA

[2]Laboratory of Retrovirology, The Rockefeller University, New York, NY, USA

[3]Department of Infectious Diseases and Respiratory Medicine, Charité-Universitätsmedizin Berlin, Berlin, Germany

[4]Howard Hughes Medical Institute, The Rockefeller University, New York, NY, USA

[5]Berlin Institute of Health (BIH), Berlin, Germany

*equal contribution

Address correspondence to: Michel C. Nussenzweig nussen@rockefeller.edu or Christian Gaebler cgaebler01@rockefeller.edu

Abstract

The SARS-CoV-2 pandemic prompted a global vaccination effort and the development of numerous COVID-19 vaccines at an unprecedented scale and pace. As a result, current COVID-19 vaccination regimens comprise diverse vaccine modalities, immunogen combinations and dosing intervals. Here, we compare vaccine-specific antibody and memory B cell responses following two-dose mRNA, single-dose Ad26.COV2.S and two-dose ChAdOx1 or combination ChAdOx1/mRNA vaccination. Plasma neutralizing activity as well as the magnitude, clonal composition and antibody maturation of the RBD-specific memory B cell compartment showed substantial differences between the vaccination regimens. While individual monoclonal antibodies derived from memory B cells exhibited similar binding affinities and neutralizing potency against Wuhan-Hu-1 SARS-CoV-2, there were significant differences in epitope specificity and neutralizing breadth against viral variants of concern. Although the ChAdOx1 vaccine was inferior to mRNA and Ad26.COV2.S in several respects, biochemical and structural analyses revealed enrichment in a subgroup of memory B cell neutralizing antibodies with distinct RBD-binding properties resulting in remarkable potency and breadth.

Introduction

Coronavirus disease-2019 (COVID-19) vaccine programs are a historic public health success that saved countless lives and prevented millions of Severe Acute Respiratory Syndrome Coronavirus (SARS-CoV-2) infections (Vilches et al., 2022). Vaccination is a multifaceted global effort involving a diverse collection of vaccine platforms including mRNA, adenoviral vector-based, inactivated virus and recombinant protein immunogens (Mathieu et al., 2021). Detailed evaluation of the different vaccine-specific immune responses will inform improved

2

49   vaccination strategies for the prevention of COVID-19 and other respiratory viral infections of

50   pandemic potential (Zhang et al., 2022).

51

52   With close to 2.5 billion administered doses, the ChAdOx1 nCoV-19 (AZD1222) vaccine

53   accounted for over one third of all global COVID-19 vaccine doses administered in 2021

54   (Mallapaty et al., 2021; Mathieu et al., 2021). The ChAdOx1 vaccine encodes full-length wild-

55   type (Wuhan-Hu-1) SARS-CoV-2 spike protein without the prefusion-stabilizing mutations

56   found in the three US-approved vaccines (BNT162b2, mRNA-1273, and Ad26.COV2.S)

57   (Watanabe et al., 2021). Outside of the US, ChAdOx1 received regulatory approval as a two-

58   dose vaccine administered at an interval of 4–12 weeks. Unfortunately, ChAdOx1 vaccination

59   was associated with immune thrombocytopenia, a rare but serious complication that has been

60   described after administration of adenoviral vector vaccines. As a result, many individuals

61   receiving a ChAdOx1 prime were subsequently boosted with an mRNA vaccine (Klok et al.,

62   2022).

63

64   The combination (ChAdOx1/mRNA vaccine) prime-boost regimen showed enhanced

65   immunogenicity (Barros-Martins et al., 2021; Hillus et al., 2021; Normark et al., 2021; Schmidt

66   et al., 2021b), however both ChadOx1-based vaccine regimens proved to be effective with

67   substantial protection against COVID-19 hospitalization and death (Andrews et al., 2022;

68   Nordstrom et al., 2021).

69

70   In-depth analyses of antibody and memory B cell responses after natural infection, mRNA

71   (BNT162b2, mRNA-1273) and Janssen Ad26.COV2.S vaccination have been performed (Cho et

72   al., 2021; Gaebler et al., 2021; Muecksch et al., 2022; Robbiani et al., 2020; Wang et al., 2021c;

73   Wang et al., 2021d). However, far less is known about the responses elicited by the ChadOx1

74   vaccine even though it was used in more countries that any other COVID-19 vaccine (Mathieu et

75   al., 2021). Here, we compare vaccine-specific antibody and memory B cell responses to 2-dose

76   mRNA (BNT162b2 or mRNA-1273), 1-dose Janssen Ad26.COV2.S, 2-dose ChAdOx1 (AZ/AZ)

77   or ChAdOx1/BNT162b2 combination (AZ/BNT) vaccines.

78

79   **Results**

80   Four cohorts of study participants with different vaccination regimens were recruited and

81   sampled prospectively. All cohorts included sampling time points at approximately 1 and 6

82   months after the 1st vaccine dose. An additional sampling time point at 1 month after 2nd

83   vaccination was available for the mRNA (1.3m after 2nd dose=2.3m after 1st dose), AZ/BNT and

84   AZ/AZ (1m after 2nd dose=4m after 1st dose) 2-dose vaccination regimens. The vaccination and

85   blood collection schedule for all cohorts in this study is depicted in Fig. 1a.

86   For the AZ/BNT and AZ/AZ cohort a total of 49 health-care workers with no prior history of

87   SARS-CoV-2-infection who received a ChAdOx1 vaccine prime followed by ChAdOx1 or

88   BNT162b2 boost 10–12-weeks later were enrolled in a prospective observational cohort study in

89   Berlin (Germany) (Hillus et al., 2021). 23 and 26 study participants received ChAdOx1 or

90   mRNA as a second dose, respectively. Volunteers ranged in age from 20-65 years and were 65%

91   female. For detailed demographic information, see Methods and Table S1 and (Cho et al., 2022;

92   Muecksch et al., 2022).

93

94   **Plasma binding and Neutralization**

4

95   Plasma antibody binding titers to SARS-CoV-2 RBD were measured by enzyme-linked

96   immunosorbent assays (ELISA) (Cho et al., 2021; Wang et al., 2021c). RBD-binding IgG levels

97   1 month after ChAdOx1 prime were lower but not significantly different to antibody levels

98   following a single dose of an mRNA vaccine (Cho et al., 2021) or the Janssen Ad26.COV2.S

99   vaccine (Cho et al., 2022) at similar time points (Fig. 1b-c). ChAdOx1 and mRNA boosting

100   enhanced IgG titers 12-fold (AZ/BNT) and 2.6-fold (AZ/AZ) 1 month after the 2nd vaccine dose,

101   respectively (p<0.0001, Fig. 1b, d). In both cases, anti-RBD antibodies in plasma decreased

102   significantly between 4 and 6 months (AZ/BNT: 3.2-fold, p<0.0001; AZ/AZ: 1.5-fold, p=0.0022,

103   Fig.1b), but antibodies binding to RBD following combination AZ/BNT vaccination remained

104   significantly higher 6 months after the initial priming dose (p<0.0001, Fig. 1b). Anti-RBD IgG

105   levels after the AZ/BNT boost were directly correlated with initial antibody levels after the prime

106   (Fig. S1a, r=0.50, p=0.012). Consistent with other reports (Barros-Martins et al., 2021; Kaku et

107   al., 2022; Pozzetto et al., 2021), AZ/BNT vaccinees exhibited anti-RBD plasma reactivity 6

108   months after the initial prime that were comparable to individuals who received two doses of an

109   mRNA vaccine (Fig. 1d, e). By contrast, antibody levels following AZ/AZ vaccination remained

110   substantially lower compared to individuals who received two doses of an mRNA vaccine.

111   Nevertheless, individuals who received AZ/AZ vaccination showed serum antibody levels that

112   exceeded those of Janssen Ad26.COV2.S vaccinees at 6m post-vaccination (Fig. 1e). In contrast

113   to IgG, AZ/BNT and AZ/AZ vaccination induced similar IgM and IgA anti-RBD antibody levels

114   (Fig. S1b-c).

115

116   RBD-binding IgG titers were negatively correlated with age 4 month after the initial prime for

117   AZ/AZ, but not AZ/BNT vaccination (r=-0.51, P=0.015, Fig. S1d-e). There were no sex-related

118   differences in antibody levels following AZ/BNT or AZ/AZ vaccination (Fig. S1f). Notably, 4

119   months after the initial prime, antibody levels in AZ/BNT vaccinees were negatively correlated

120   with the interval between prime and 2nd vaccination, suggesting that earlier administration of a

121   heterologous booster vaccination may result in optimal protection (r=-0.50, P=0.010, Fig. S1g-

122   h).

123

124   Neutralizing activity was determined for the same participants, using HIV-1 pseudotyped with

125   Wuhan-Hu-1 SARS-CoV-2 spike (S) protein (Robbiani et al., 2020; Schmidt et al., 2020) (Table

126   S1).

127   The geometric mean half-maximal neutralizing titer (NT50) 1 month after the ChAdOx1 initial

128   prime were comparable to a single dose of an mRNA vaccine (Cho et al., 2021) or Janssen

129   Ad26.COV2.S (Cho et al., 2022) vaccine (Fig. 1f, g). Administration of a second dose increased

130   NT50s among AZ/BNT and AZ/AZ vaccinees from 139 to 1946 and 305, respectively

131   (p<0.0001, Fig.1f). In line with the greater initial neutralizing activity, the decrease between 4-6

132   months after the initial prime was more pronounced among combination AZ/BNT than AZ/AZ

133   vaccinees (4.6-fold, p<0.0001 vs. 1.8- fold, p=0.0066 respectively, Fig.1f). Nevertheless,

134   compared to AZ/AZ vaccinees, plasma neutralizing activity remained significantly higher 6

135   months after the initial prime in AZ/BNT vaccinees (p=0.01, Fig. 1f)

136

137   Consistent with ELISA reactivity, AZ/BNT elicited similar neutralizing activity as two doses of

138   an mRNA vaccine 6 months after the initial prime (Fig. 1h). By contrast, plasma neutralizing

139   activity after AZ/AZ vaccination was substantially lower than in individuals who received two

140   doses of an mRNA vaccine but exceeded neutralizing titers of individuals that received a single

141   dose of the Janssen Ad26.COV2.S vaccine (Fig. 1h, i).

142

143   Plasma neutralizing activity for 24 randomly selected samples (n=12, AZ/BNT; n=12, AZ/AZ)

144   was also assessed against SARS-CoV-2 Delta and Omicron BA.1 variants using viruses

145   pseudotyped with appropriate variant spikes (Cho et al., 2021; Schmidt et al., 2021a; Schmidt et

146   al., 2020; Wang et al., 2021d). Four months after the initial AZ/BNT prime vaccination,

147   neutralizing titers against Delta and Omicron BA.1 were 5.5-, and 11.6-fold lower than against

148   Wuhan-Hu-1, with a further decrease to 5.6- and 13.6-fold lower activity at the 6-month time

149   point respectively (Fig. 1j-k and Fig. S1i). Similarly, AZ/AZ vaccination resulted in 5.8- and 21-

150   fold lower neutralizing activity against Delta and Omicron BA.1 than against Wuhan-Hu-1

151   respectively at the 4-month time point. While Delta neutralization further decreased 6.4-fold

152   compared to Wuhan-Hu-1 at the 6-month time point, the neutralizing activity against Omicron

153   BA.1, which was initially very low, decreased to a lesser extent among AZ/AZ vaccinees (Fig.

154   1j-k, Fig. S1i-k).

155

156   Remarkably, 1 month after the 2nd vaccine dose Omicron BA.1 neutralizing titers in combination

157   AZ/BNT vaccinees exceeded neutralizing activity after AZ/AZ or 2-dose mRNA vaccination at

158   similar time points by 6.4- and 10.3-fold, respectively (p=0.003 and p<0.0001 Fig. 1l). Omicron

159   BA.1 neutralizing titers remained higher in AZ/BNT vaccinees, but were not statistically

160   different from mRNA, or AZ/AZ vaccinees 6 months after the prime, while titers in Janssen

161   Ad26.COV2.S vaccinees were significantly lower (Fig. 1m).

162

7

Memory B cell responses to SARS-CoV-2 RBD and NTD

To compare the development of B cell memory after COVID-19 vaccination, we initially

enumerated memory B cells expressing surface receptors binding to the Receptor-Binding

Domain (RBD) and N-Terminal Domain (NTD) of the SARS-CoV-2 spike protein using

fluorescently labeled proteins (Fig. 2a, Fig. S2a-d). The number of RBD-binding memory B cells

found in circulation 1 month after AZ prime was significantly lower than after mRNA

(p<0.0001, (Bednarski et al., 2022; Cho et al., 2021)) and Janssen Ad26.COV2.S vaccination

(p=0.0029 (Cho et al., 2022)) (Fig. 2b). Although the number of RBD-binding memory B cells

increased after AZ/BNT or AZ/AZ boosting (Fig. 2c), the number remained lower than after 2-

dose mRNA vaccination (AZ/BNT: p=0.02, AZ/AZ: p=0.0003, Fig. 2d). By contrast, the number

of NTD-binding memory B cells remained unchanged after the 2nd dose (Fig. S2c-d) and was

similar to 2-dose mRNA and significantly lower than in Janssen Ad26.COV2.S vaccinees 6

months post vaccination (AZ/BNT: p=0.0007; AZ/AZ: p=0.0001, Fig. S2e).

To examine the specificity and neutralizing activity of the antibodies produced by memory cells

we purified single Wuhan-Hu-1 RBD-specific B cells, sequenced their antibody genes, and

produced the recombinant antibodies *in vitro*. 450 paired anti-RBD antibody sequences were

obtained from 22 vaccinees (AZ/BNT n=10; AZ/AZ n=12) sampled 6 months after the initial

prime (Fig. 2e, and Fig. S2f-g, Fig. S3, Table S2). Clonally expanded RBD-specific B cells

across the different vaccine regimens 6 months after prime represented 23%, 13%, 22% and 16%

of all memory cells from mRNA, Janssen Ad26.COV2.S, AZ/BNT and AZ/AZ vaccinees,

respectively (Fig. 2e). Similar to mRNA and Janssen Ad26.COV2.S vaccinees, VH3-30, VH1-46

and VH3-53 genes were overrepresented among AZ/BNT and AZ/AZ vaccinees (Fig. S4, (Cho

186 et al., 2021; Cho et al., 2022)). There was no difference in the number of somatic mutations

187 between AZ/BNT or AZ/AZ vaccinees, although both groups showed significantly lower

188 accumulation of somatic mutations than mRNA or Janssen Ad26.COV2.S vaccinees assayed at

189 similar timepoints (p<0.0001, Fig. 2f).

190

191 We conclude that there are substantial differences in the magnitude, clonal composition, and

192 antibody maturation of the RBD-specific memory B cell compartment between the different

193 vaccination regimens. However, homologous and combination booster vaccination after a

194 ChAdOx1 prime are not significantly different with respect to the number of memory B cells that

195 develop, or their levels of somatic mutation.

196

197 **Neutralizing activity of monoclonal antibodies**

198 Next, we compared the neutralizing activity of monoclonal antibodies elicited by mRNA,

199 Janssen Ad26.COV2.S, and AZ/BNT or AZ/AZ vaccination. 291 anti-RBD monoclonal

200 antibodies were expressed and tested for binding by ELISA. 94% (n=277) bound to the Wuhan-

201 Hu-1 RBD, indicating the high efficiency of RBD-specific memory B cell isolation (Table S3).

202 The geometric mean ELISA half-maximal concentration (EC_{50}) of the RBD-binding monoclonal

203 antibodies elicited by AZ/AZ or AZ/BNT vaccination was comparable (Fig. 3a). EC_{50}s represent

204 an indirect measure of affinity. To directly examine anti-RBD antibody affinity, we performed

205 biolayer interferometry (BLI) experiments on a subset of antibodies (n=66 from AZ/BNT and

206 n=62 from AZ/AZ). Affinity was comparable among antibodies elicited by mRNA, Janssen

207 Ad26.COV2.S, and AZ/BNT or AZ/AZ vaccination (Fig. 3b, (Cho et al., 2021)). All 277 RBD-

208 binding IgG monoclonal antibodies were tested for neutralization against viruses pseudotyped

9

209   with Wuhan-Hu-1 SARS-CoV-2 spike protein (183 and 94 antibodies isolated from AZ/BNT

210   and AZ/AZ vaccinees, respectively). Memory B cell antibodies elicited by mRNA, Janssen

211   Ad26.COV2.S, AZ/BNT and AZ/AZ vaccination 6 months after the prime showed comparable

212   activity (Fig 3c). Similarly, the proportion of neutralizing to non-neutralizing antibodies for all

213   four regimens was not significantly different (Fig. 3d). We conclude that memory B cells present

214   in circulation 6 months after initial mRNA, Janssen Ad26.COV2.S, AZ/AZ and AZ/BNT

215   vaccine doses express antibodies with similar binding affinities and neutralizing potency against

216   Wuhan-Hu-1 SARS-CoV-2.

217

218   **Epitopes and Neutralizing Breadth**

219   SARS-CoV-2 infection and vaccination elicit anti-RBD antibodies that target four structurally

220   defined classes of epitopes on the RBD (Barnes et al., 2020; Muecksch et al., 2022; Muecksch et

221   al., 2021; Wang et al., 2021c; Yuan et al., 2020). Class 1 and 2 antibodies block ACE2 binding

222   directly, and Class 3 and 4 antibodies target more conserved regions on the RBD (Gaebler et al.,

223   2021; Muecksch et al., 2022; Muecksch et al., 2021; Wang et al., 2021c). Class 1 and 2

224   antibodies develop early after infection or mRNA-immunization (Muecksch et al., 2022), while

225   Janssen Ad26.COV2.S vaccination leads to a more diverse, early memory B cell response that is

226   dominated by Class 3 and 4 antibodies (Cho et al., 2022). Nevertheless, continued memory B

227   cell evolution results in comparable epitope specificities 5-6 months after the initial mRNA or

228   Janssen Ad26.COV2.S immunization (Cho et al., 2022).

229

230   To define the epitopes recognized by anti-RBD memory antibodies elicited by AZ/BNT or

231   AZ/AZ vaccination, we performed BLI competition experiments. A preformed antibody-RBD-

10

232 complex was exposed to a second antibody targeting one of four classes of structurally defined

233 epitopes (Barnes et al., 2020; Robbiani et al., 2020) (C105 as Class 1; C144 as Class 2; C135 as

234 Class 3; and CR3022 as Class 4). We examined 128 RBD-binding antibodies randomly obtained

235 from the AZ/BNT (n=66) and AZ/AZ (n=62) vaccinees. This included AZ/BNT (n=44) and

236 AZ/AZ (n=39) antibodies with IC_{50}s less than 1000 ng/mL.

237

238 The epitope distribution of the memory antibody repertoires was significantly different between

239 all four vaccine regimens (Fig. S5a). Moreover, the overall epitope specificities of the antibody

240 repertoires were significantly different between mRNA vaccinees and AZ/BNT or AZ/AZ

241 vaccinees (Fig. 4a). This was particularly evident among neutralizing (IC_{50}<1000ng/ml)

242 antibodies for which the frequency of antibodies that target unknown epitopes (non-classified)

243 was highly enriched in the antibody repertoire isolated from AZ/BNT or AZ/AZ vaccinees (Fig.

244 4a). At the same time, there were no significant differences in epitope specificities for non-

245 neutralizing (IC_{50}>1000 ng/ml) antibodies.

246

247 To examine the contribution of the different antibody classes to the neutralizing potency and

248 breadth elicited by each of the four vaccine regimens, we regrouped the antibodies as follows: 1)

249 Antibodies targeting Class 1 and/or 2 epitopes; 2) antibodies additionally or exclusively targeting

250 Class 3 epitopes; 3) antibodies additionally or exclusively targeting Class 4 epitopes; or 4) non-

251 classifiable antibodies. While neutralizing potency of the first 3 groups was comparable among

252 all four vaccines regimens, AZ/BNT and AZ/AZ vaccination elicited non-classifiable antibodies

253 that were significantly more potent than their mRNA or Janssen counterparts (Fig. 4b).

254

11

255   To determine the neutralizing breadth of the memory antibodies that developed after AZ/BNT or

256   AZ/AZ vaccination, we analyzed a panel of randomly selected Wuhan-Hu-1 (WT)-neutralizing

257   antibodies from AZ/BNT and AZ/AZ vaccinees (AZ/BNT: n=32, and AZ/AZ: n=34) for

258   neutralizing activity against SARS-CoV-2 pseudoviruses carrying amino acid substitutions

259   specific to the Delta- and Omicron BA.1-RBD.

260

261   78% of the AZ/BNT- and 82% of the AZ/AZ-elicited antibodies neutralized SARS-CoV-2

262   pseudoviruses carrying the Delta RBD-amino acid substitutions, some with IC_{50} values of less

263   than 10 ng/ml (Fig. 4c and Table S4). Omicron BA.1 showed the highest degree of neutralization

264   resistance, nevertheless 8 out of 32 antibodies isolated from AZ/BNT and 14 out of 34 antibodies

265   isolated from AZ/AZ vaccinees neutralized this variant. Some of the most potent Omicron-

266   neutralizing antibodies targeted epitopes that could not be classified in our BLI experiments

267   (non-classified) with IC_{50}s below 10 ng/ml (Fig. 4c-d and Table S4). 5 out of 32 AZ/BNT- and

268   10 out of 34 AZ/AZ- antibodies neutralized both Delta and Omicron, a proportion that was not

269   significantly different compared to antibodies elicited by other vaccine regimens (Fig. 4c and e).

270

271   We conclude that the relative distribution of RBD epitopes targeted by neutralizing antibodies

272   expressed by memory B cells that develop after mRNA, Janssen Ad26.COV2.S or ChAdOx1

273   vaccination regimens differ significantly.

274

275   **Structural analysis of antibody-RBD interaction**

276   To understand the interaction between these none-classified antibodies and RBD, we imaged WT

277   Wuhan-Hu-1 SARS-CoV-2 S 6P bound to Fab fragments of a potent and broad AZ/AZ antibody

278   (AZ090) by single-particle cryo-electron microscopy (cryo-EM) (Fig. 5a and Fig. S6). The

279   resolution of the reconstituted cryo-EM electron density map was 3 Å for the whole complex and

280   the spike-AZ090. Structural analyses of the density maps showed that the binding orientation of

281   AZ090 is similar to previously described potent antibodies that were isolated following natural

282   infection (Dejnirattisai et al., 2021; Reincke et al., 2022; Tortorici et al., 2020; Wang et al.,

283   2021a) (Fig. S7). AZ090 and this type of antibodies share the same immunoglobulin heavy and

284   light chain genes (IGHV1-58 and IGKV3-20/IGKJ) (Fig. S7). Unlike Class 1 antibodies, the

285   footprint of AZ90 is located in the ridge region of RBD with more limited overlap with Omicron

286   (BA.1) amino acid substitutions than typical class 1 (C105) and class 2 (C144) antibodies (Fig.

287   5b). The distinctive binding pattern of AZ090 may also explain the lack of competition in BLI

288   experiments and the neutralizing breadth across different SARS-CoV-2 variants.

289

Discussion

291   Neutralizing antibodies are correlates of vaccine efficacy in protection against SARS-CoV-2

292   infection and severe COVID-19 (Bergwerk et al., 2021; Feng et al., 2021; Khoury et al., 2021; Li

293   et al., 2022). All three US-authorized vaccines have shown substantial protection against SARS-

294   CoV-2 infection, hospitalization, and death (Botton et al., 2022; Self et al., 2021). However,

295   vaccine efficacy wanes over time with prominent loss of protection against infection after the

296   Janssen Ad26.COV2.S vaccine compared to mRNA (Lin et al., 2022). Similarly, vaccination

297   regimens with the globally predominant ChAdOx1vaccine have been less effective in the

298   protection against infection and symptomatic COVID-19 compared to mRNA vaccination

299   (Andrews et al., 2022; Braeye et al., 2022). However, the combination of a ChAdOx1 prime and

13

300   a 2nd mRNA dose shows similar levels of protection as 2-dose mRNA vaccination (Nordstrom et

301   al., 2021).

302

303   Our comparative analysis of plasma and memory B cell antibodies provides a mechanistic

304   explanation for the observed real-world protective efficacy of the several different vaccine

305   regimens. Binding and neutralizing antibody levels elicited by 2-dose mRNA or AZ/BNT

306   vaccination exceeds those elicited by AZ/AZ or single-dose Janssen Ad26.COV2.S vaccination.

307   Omicron BA.1 neutralization was highest after AZ/BNT vaccination suggesting that combination

308   vaccine protocols with extended dosing intervals may induce improved plasma neutralizing

309   responses. In line with our observation, vaccine efficacy has been shown to increase with the

310   interval between the 1st and 2nd vaccine dose (Voysey et al., 2021). Prolonged affinity maturation

311   yielding higher affinity B cells for plasma cell maturation upon the administration of the 2nd

312   vaccine dose may be of importance in this process (Hall et al., 2022).

313

314   The relative potency and breadth, i.e. neutralizing activity against Delta and Omicron, of

315   memory B cell antibodies produced by the 4 different vaccine regimens was overall similar.

316   However, they differed in the absolute number of memory cells and the distribution of the RBD

317   epitopes targeted by mRNA, Janssen Ad26.COV2.S and ChAdOx1 vaccination regimens.

318   Differences in dosing intervals between prime and boost immunization, distinct antigenic

319   features of the full-length wild-type SARS-CoV-2 spike protein lacking prefusion-stabilizing

320   mutations in the ChAdOx1 vaccine (Tortorici and Veesler, 2019), and the precise biochemistry

321   of the antigen and its presentation may all contribute to these observations.

322

323   Notably, the number of RBD-binding memory cells that develop after 2-dose mRNA vaccination

324   is greater than vaccination regimens that are based on adenoviral vectors. The latter is likely to

325   be particularly important for recall responses and protection from severe diseases upon repeated

326   viral challenge (Amanna et al., 2007; Mesin et al., 2020).

327

328   **FIGURES**
329   **Fig.1**

330

16
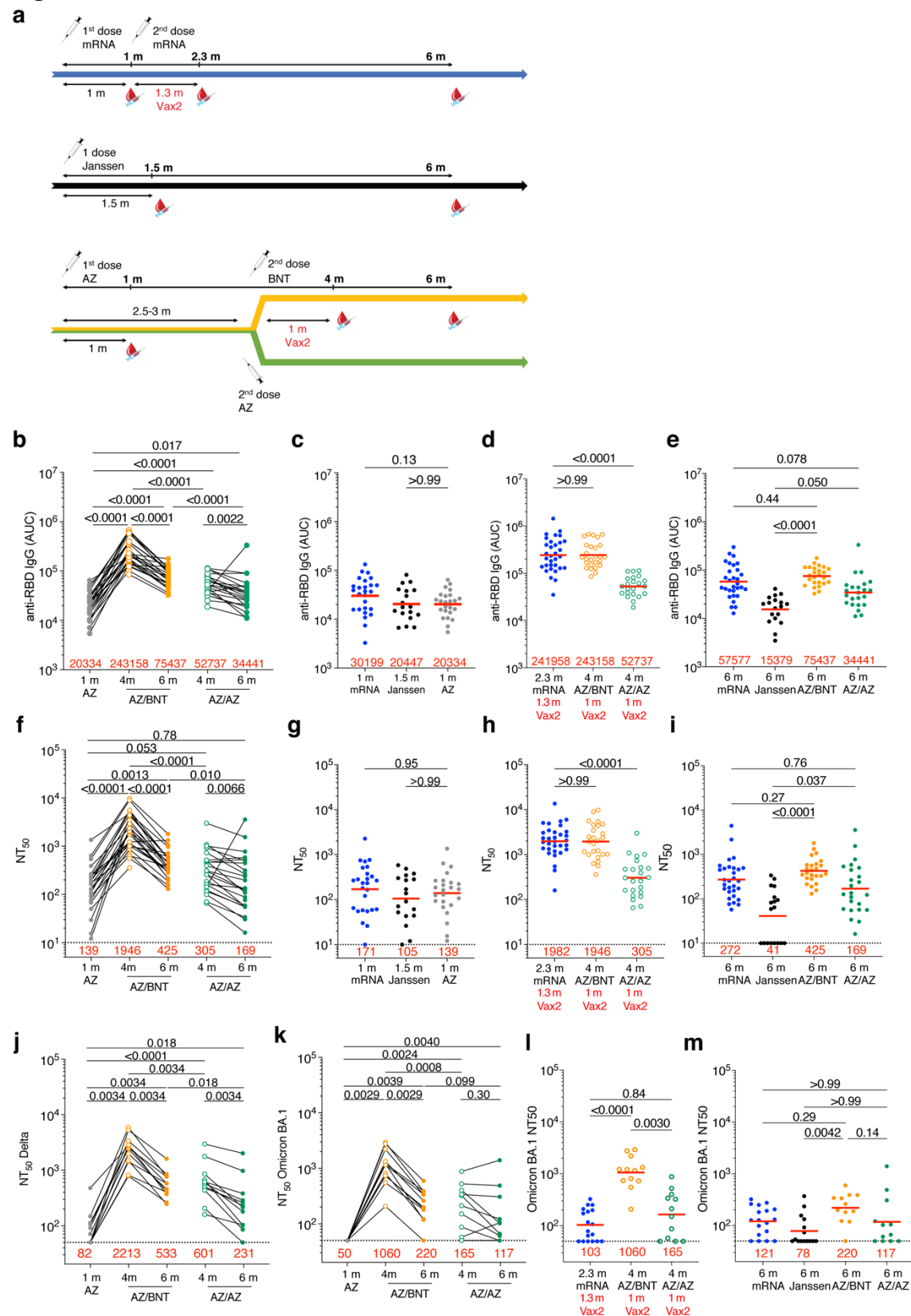
Fig. 1: Plasma binding and neutralizing activity.

a, Vaccination and blood donation schedules for mRNA vaccinees (upper panel), Ad26.COV.2S (Janssen) vaccinees (middle panel), and ChAdOx1 (AZ) vaccinees boosted with either BNT162b2 (BNT, upper half of lower panel) or AZ (lower half of lower panel). **b,** Area under the curve (AUC) for plasma IgG antibody binding to SARS-CoV-2 Wuhan-Hu-1 RBD 1 month (m) after mRNA prime (Cho et al., 2021), or Janssen Ad26.COV.2S prime (Cho et al., 2022) or AZ prime, as well as 4 months or 6 months after the initial AZ prime (AZ/BNT; n=26) or (AZ/AZ; n=23). Lines connect longitudinal samples. **c-e,** AUC for plasma IgG binding to Wuhan-Hu-1 RBD in vaccinees 1 m after AZ prime compared to mRNA prime (Cho et al., 2021) or Janssen Ad26.COV2.S (Cho et al., 2022) prime at similar timepoint **(c)** , mRNA vaccinees 2.3 m after initial dose (Cho et al., 2021) compared to AZ/BNT and AZ/AZ vaccinees 4 m after initial dose **(d)**, or mRNA vaccinees 6 m after initial dose (Cho et al., 2021) and Janssen Ad26.COV2.S vaccinees 6 m after one dose (Cho et al., 2022) compared to AZ/BNT and AZ/AZ vaccinees 6 m after initial dose **(e)**. **f-i,** Anti-SARS-CoV-2 NT_{50}s of plasma measured by a SARS-CoV-2 pseudotype virus neutralization assay using wild-type (Wuhan-Hu-1 (Wu et al., 2020)) SARS-CoV-2 pseudovirus (Robbiani et al., 2020; Schmidt et al., 2020) in plasma samples shown in panels **a-e**. **j-m,** Plasma neutralizing activity against indicated SARS-CoV-2 Delta **(j)** and Omicron **(k)** variants for n=24 (AZ/BNT: n=12 and AZ/AZ:n=12) randomly selected samples assayed in HT1080Ace2 cl.14 cells. **l-m,** mRNA vaccinees 2.3 m after initial dose (Cho et al., 2021) compared to AZ/BNT and AZ/AZ vaccinees 4 m after initial dose **(l)**, or mRNA vaccinees 6 m (Cho et al., 2021) and Janssen Ad26.COV2.S vaccinees 6 m after initial dose (Cho et al., 2022) compared to AZ/BNT and AZ/AZ vaccinees 6 m after initial dose **(m)**. See Methods for a list of all substitutions/deletions/insertions in the spike variants. Deletions/substitutions corresponding to viral variants were incorporated into a spike

354   protein that also includes the R683G substitution, which disrupts the furin cleavage site and

355   increases particle infectivity. All experiments were performed at least in duplicate. Red bars and

356   values represent geometric mean values. Statistical significance was determined by two-tailed

357   Mann-Whitney test for unpaired observations or by Wilcoxon matched-pairs signed rank test for

358   paired observations followed by Holm-Šídák test for multiple comparisons (**a, f, j-k**), two-tailed

359   Kruskal-Wallis test with subsequent Dunn's multiple comparisons (**b-e, g-I, l-m**).

360

361   **Fig.2**

362
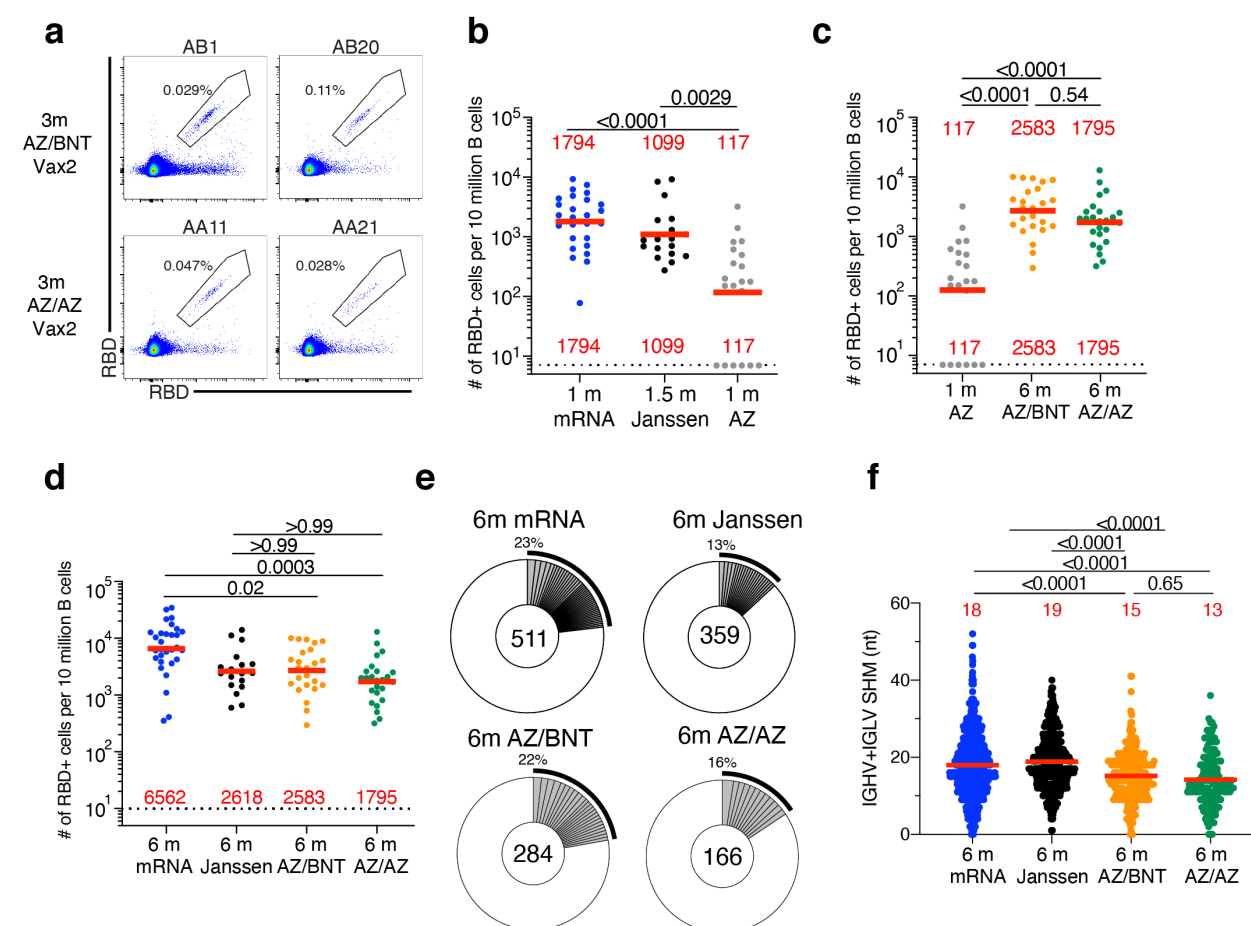
363   **Fig. 2: Anti-SARS-CoV-2 RBD B cell memory. a,** Representative flow cytometry plots showing

18

364   dual AlexaFluor-647- and PE-Wuhan-Hu-1-RBD-binding single sorted B cells from

365   ChAdOx1/BNT162b2 (AZ/BNT, n=2) and ChAdOx1/ChAdOx1 (AZ/AZ, n=2) vaccinees 6

366   months (m) after initial dose. Gating strategy shown in **Fig. S2**. Percentage of antigen-specific B

367   cells is indicated. **b,** Number of Wuhan-Hu-1 RBD-specific B cells per 10 million (M) B cells in

368   mRNA vaccinees 1 m after prime (Cho et al., 2021) and Ad26.COV.2S (Janssen) vaccinees 1.5 m

369   after prime (Cho et al., 2022) compared to AZ vaccinees 1 m after prime. **c,** Number of Wuhan-

370   Hu-1 RBD-specific B cells per 10 M B cells for AZ vaccinees 1 m after prime compared to

371   AZ/BNT and AZ/AZ vaccinees 6 m after initial dose. **d,** Number of Wuhan-Hu-1 RBD-specific B

372   cells per 10 M B cells for mRNA vaccinees 6 m after initial dose (Cho et al., 2021) and Janssen

373   Ad26.COV2.S vaccinees 6 m after prime (Cho et al., 2022) compared to AZ/BNT and AZ/AZ

374   vaccinees 6 m after initial dose. **e,** Pie charts show the distribution of antibody sequences obtained

375   from Wuhan-Hu-1 RBD-specific memory B cells of mRNA vaccinees 6 m after initial dose and

376   Ad26.COV.2S (Janssen) vaccinees 6 m after initial prime, or AZ/BNT and AZ/AZ vaccinees 6 m

377   after initial dose. The number inside the circle indicates the aggregate number of sequences

378   analyzed for each cohort. Grey slices indicate expanded clones (same *IGHV* and *IGLV* genes with

379   highly similar CDR3s, see Methods) found within the same individual. Pie slice size is

380   proportional to the number of clonally related sequences. The black outline and associated

381   numbers indicate the total percentage of clonally expanded sequences. **f,** Number of nucleotide

382   somatic hypermutations (SHM) in *IGHV + IGLV* sequences obtained from Wuhan-Hu-1 RBD-

383   specific memory B cells of mRNA vaccinees 6 m after initial dose and Janssen Ad26.COV2.S

384   vaccinees 6 m after prime compared to AZ/BNT and AZ/AZ vaccinees 6 m after initial dose. Red

385   bars and numbers in **b, c**, and d represent geometric mean value, and in f represent mean values.

386   Statistical difference in **b, c, d** and **f**, was determined by two-tailed Kruskal Wallis test with

387   subsequent Dunn's multiple comparisons.

388

389   **Fig.3**

390
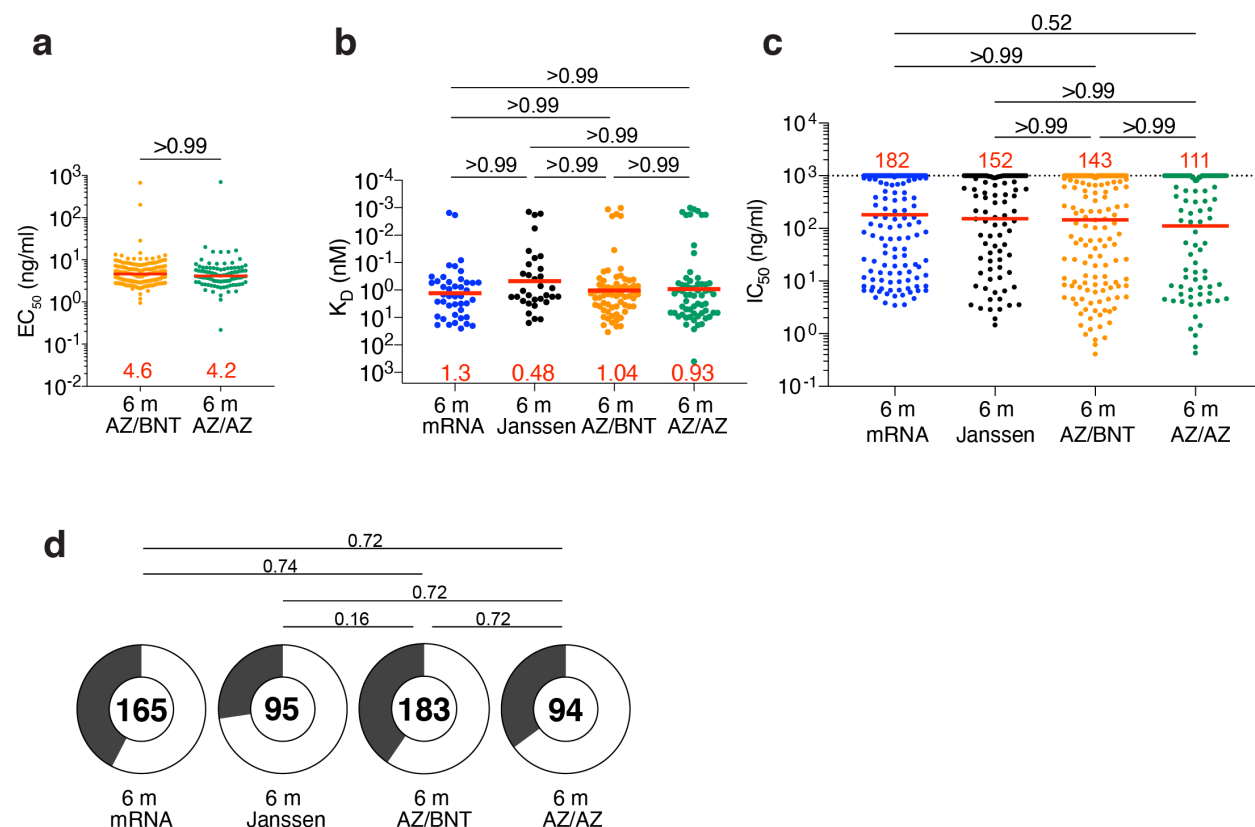
391   **Fig. 3: Anti-SARS-CoV-2 monoclonal antibodies.**

392   **a**, Graph shows half-maximal effective concentration (EC_{50}) of n=277 Wuhan-Hu-1 RBD-binding

393   monoclonal antibodies (mAbs) measured by ELISA against Wuhan-Hu-1 RBD from AZ/BNT

394   (n=183) and AZ/AZ (n=94) vaccinees. **b**, Graph showing affinity measurements (K_{D}s) for Wuhan-

395   Hu-1 RBD measured by BLI for antibodies cloned from mRNA vaccinees 6 months(m) after initial

396   dose (n=43) (Cho et al., 2021), from Janssen Ad26.COV2.S vaccinees 6 m (n=33) after prime

397   (Cho et al., 2022), compared to antibodies cloned from AZ/BNT (n=189) and AZ/AZ (n=94)

398   vaccinees 6 m after initial dose. **c**, Graphs show anti-SARS-CoV-2 neutralizing activity of

20

399   monoclonal antibodies measured by a SARS-CoV-2 pseudotype virus neutralization assay using

400   wild-type (Wuhan-Hu-1(Wu et al., 2020)) (SARS-CoV-2 pseudovirus (Robbiani et al., 2020;

401   Schmidt et al., 2020)) for antibodies cloned from mRNA vaccinees and 6 m after initial dose

402   (n=262) (Cho et al., 2021), or from Janssen Ad26.COV2.S vaccinees (n=95) 6 m after prime (Cho

403   et al., 2022), compared to antibodies cloned from AZ/BNT (n=189) and AZ/AZ (n=94) vaccinees

404   6 m after initial dose. **d**. Pie charts indicated the frequency of neutralizing ($IC_{50}<1000$ ng/mL,

405   white) vs. non-neutralizing ($IC_{50}>1000$ ng/mL, black) antibodies cloned from mRNA

406   vaccinees(Cho et al., 2021), Janssen Ad26.COV2.S vaccinees(Cho et al., 2022), AZ/AZ vaccinees

407   and AZ/BNT vaccinees. Red bars and lines indicate geometric mean values. Statistical significance

408   in a, b, and c was determined by two-tailed Kruskal Wallis test with subsequent Dunn's multiple

409   comparisons. Pie charts were compared using a two-tailed Fisher's exact test.

410

411   **Fig.4**

412

413
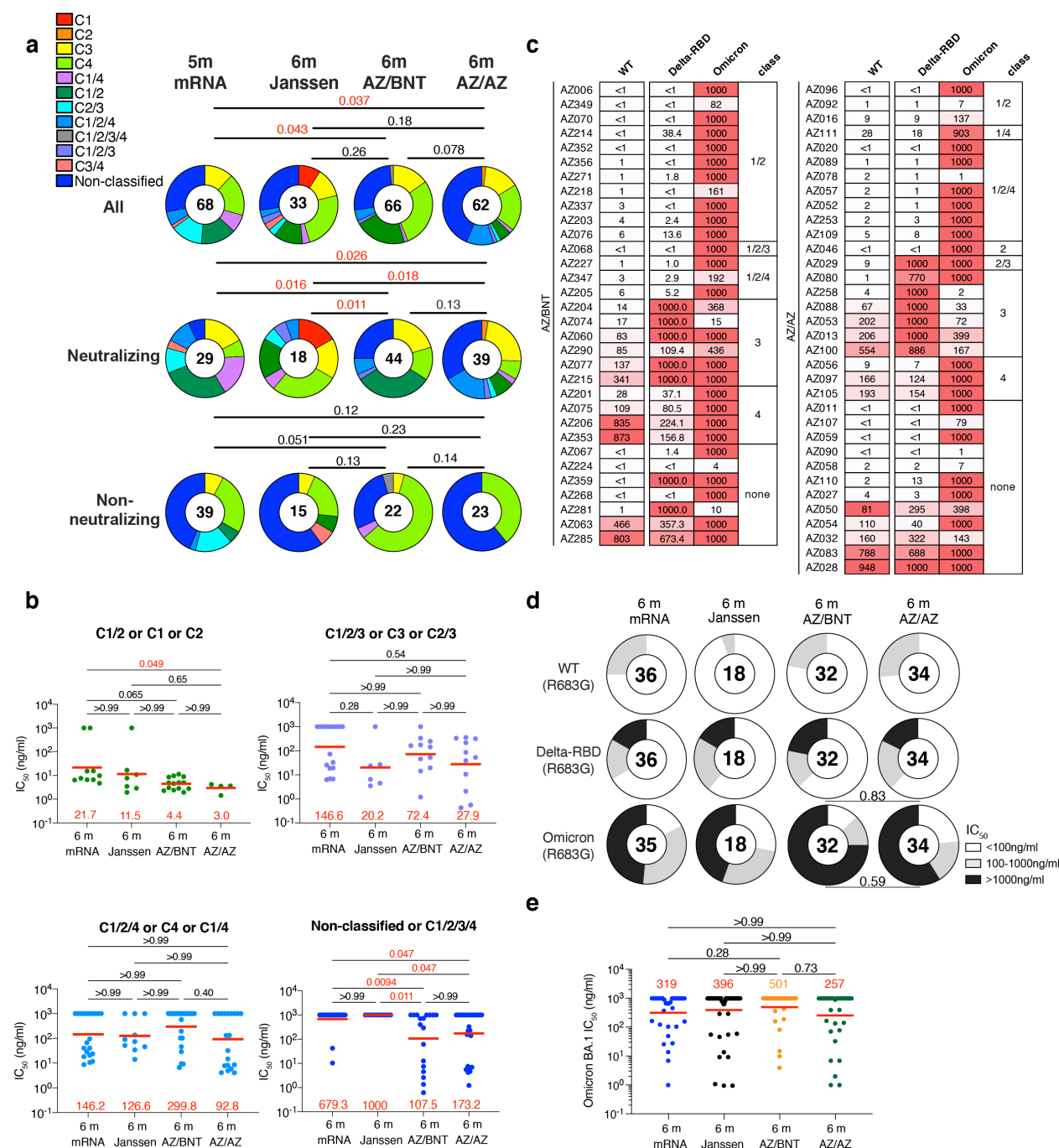
414   **Fig. 4: Epitopes and neutralizing breadth.**

415 Results of epitope mapping performed by competition BLI, comparing mAbs cloned from Janssen

416 vaccinees 6 m (n=33) after prime (Cho et al., 2022) and mAbs cloned from mRNA vaccinees 6 m

417 after initial dose (n=68) (Cho et al., 2021), to mAbs cloned from AZ/AZ (n=62) or AZ/BNT(n=66)

418 vaccinees 6 m after initial dose. **a**, Pie charts show the distribution of the antibody classes among

419 all RBD-binding antibodies, Wuhan-Hu-1 neutralizing antibodies only or non-neutralizing

420 antibodies only. Statistical significance was determined by using a two-tailed Chi-square test. **b**,

421 Graphs showing IC_{50} neutralization activity of antibodies indicated in **a** and **Fig. S5a**, with 4

422 categories by combining 1) C1/2 or C1 or C2 as C1/2; 2) C1/2/3 or C3 or C2/3 as C1/2/3; 3) C1/2/4

423 or C4 or C1/4 as C1/2/4; 4) Non-classified and C1/2/3/4 as non-classified. **c**, Heat-maps show

424 IC_{50}s of antibodies obtained from AZ/BNT vaccinees (n=32), and AZ/BNT vaccinees (n=34),

425 against indicated mutant and variant SARS-CoV-2 pseudoviruses listed across the top. Delta-RBD

426 indicate the L452R/T478K and Omicron BA.1. The deletions/substitutions corresponding to viral

427 variants were incorporated into a spike protein that also includes the R683G substitution, which

428 disrupts the furin cleavage site and increases particle infectivity. **d**. Pie charts show fraction of

429 potent neutralizing (IC_{50}<100ng/ml), less potent neutralizing (100ng/ml<IC_{50}<1000ng/ml) and

430 non-neutralizing (IC_{50}>1000 ng/ml) antibodies in white, light and dark grey, respectively, for

431 indicated SARS-CoV-2 pseudoviruses. Number in inner circles indicates number of antibodies

432 tested. **e**. Graphs showing IC_{50} neutralization activity of antibodies mAbs cloned from Janssen

433 Ad26.COV2.S vaccinees at 6 m (n=54) after prime (Cho et al., 2022) and mAbs cloned from

434 mRNA vaccinees at 6 m after initial dose (n=35) (Cho et al., 2021), to mAbs cloned from AZ/AZ

435 (n=34) or AZ/BNT(n=32) vaccinees 6 m after initial dose, against Omicron BA.1. Red bars and

436 lines indicated geometric mean values. Statistical significance in **a** was determined by two-tailed

437   Kruskal Wallis test with subsequent Dunn's multiple comparisons in **b** and **e**. Statistical

438   significance was determined using a two-tailed Chi-square test.

439

440   **Fig. 5**

441
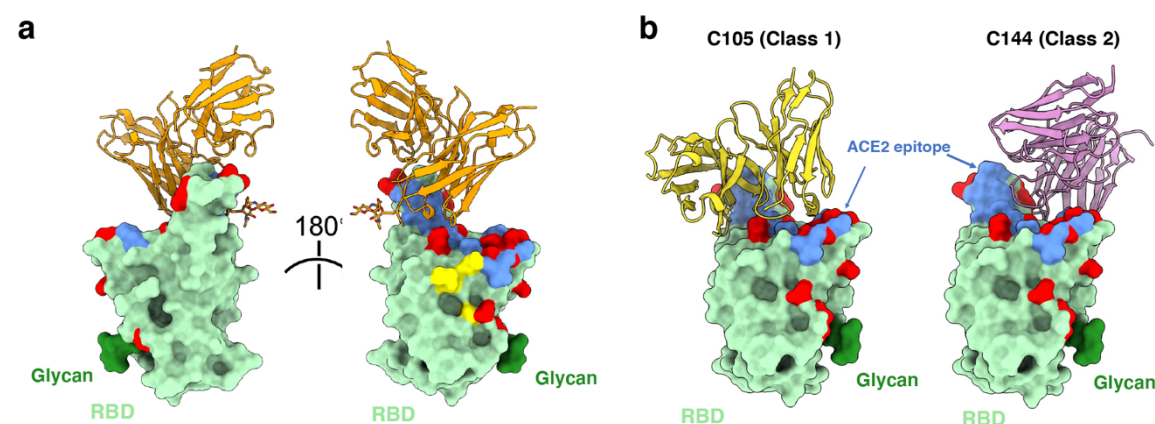
442   **Fig. 5 Structural analysis of AZ090 antibody**

443   **a**, RBDs of SARS-CoV-2 were shown by surface and colored green. RBD and AZ090 were

444   shown by cartoon and AZ090 fab was colored in orange, ACE2 epitope was colored blue and

445   N343 glycan was colored green. Omicron (BA.1) mutations were shown red. **b**, as in **a**. C105

446   (Class 1 antibody, PDB:6XCM) was colored in yellow and C144 (Class 2 antibody, PDB:7K90)

447   was colored in pink.

448

449   **Supplementary Figures**

450   **Fig. S1**
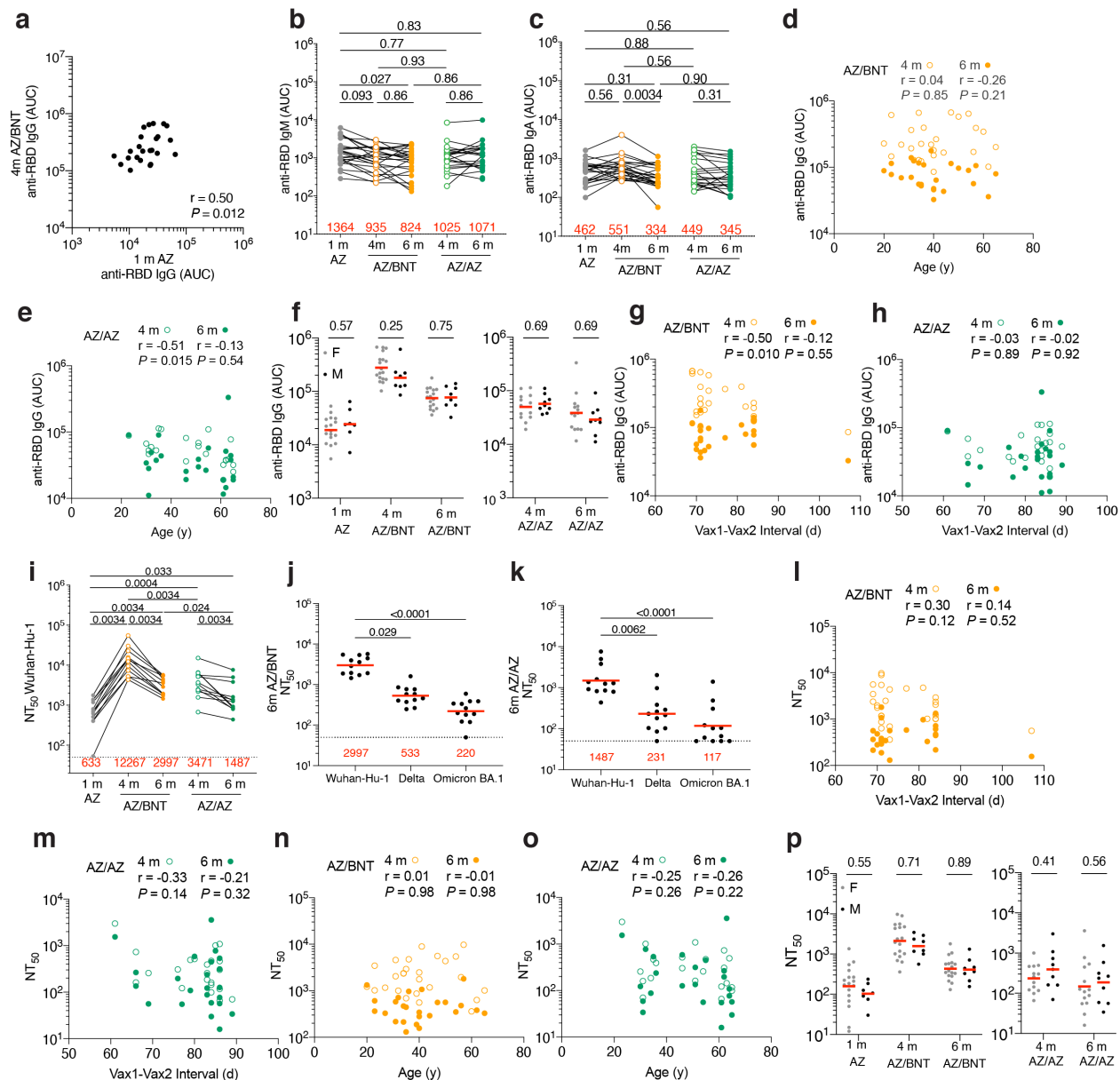
Fig. S1: Demographics and Plasma Correlations.

a, AUC for anti-RBD IgG at 1 m after ChAdOx1(AZ) prime plotted against AUC for anti-RBD IgG at 4 m after initial dose following the ChAdOx1/BNT162b2 AZ/BNT scheme. **b-c**, Area under the curve (AUC) for **b**, plasma IgM and **c**, plasma IgA antibody binding to SARS-CoV-2 Wuhan-Hu-1 RBD 1 months (m) after AZ prime, as well as 4 m and 6 m after initial dose with either BNT162b2 (AZ/BNT; n=26) or ChAdOx1 (AZ/AZ; n=23). Lines connect longitudinal samples.

458   **d-e**, Age (X axis) plotted against area under the curve (AUC) (Y axis) for anti-RBD IgG at 4 m

459   and 6 m after initial dose following **a,** the AZ/BNT scheme, or **b,** the AZ/AZ scheme. **f,** AUC for

460   anti-RBD IgG 1 m after prime, as well as 4 m and 6 m after initial dose for all male (M: n=8) or

461   women (F: n=18) vaccinated following the AZ/BNT scheme (left panel), or AUC for anti-RBD

462   IgG 4 m and 6 m after initial dose for all male (M: n=9) or female (F: n=14) following the AZ/AZ

463   scheme (right panel). **g-h,** Interval between first and second vaccination (X axis) plotted against

464   AUC for anti-RBD IgG (Y axis) at 4 m and 6 m after initial dose following **g,** the AZ/BNT scheme,

465   or **h,** the AZ/AZ scheme. **i-k,** Plasma neutralizing activity against indicated SARS-CoV-2 variants

466   of interest/concern for n=12 randomly selected samples assayed in HT1080Ace2 cl.14 cells.

467   Viruses in i-k contained the R683G furin cleavage site mutation to increase particle infectivity.

468   **(See also in Fig. 1j-m)**. **l-m**, Interval between first and second vaccination (X axis) plotted against

469   NT_{50} values (Y axis) 4 m and 6 m after initial dose following **l,** the AZ/BNT scheme, or **m,** the

470   AZ/AZ scheme. **n-o**, Age (X axis) plotted against NT_{50} values (Y axis) 4 m and 6 m after initial

471   dose following **n,** the AZ/BNT scheme, or **o,** the AZ/AZ scheme. **p**, NT_{50} values at 1 m after AZ

472   prime, as well as 4 m and 6 m after initial dose for all male (M; n=8) or female (F; n=18) following

473   the AZ/BNT scheme (left panel), or NT_{50} values at 4 m and 6 m after initial dose for all male (M;

474   n=9) or female (F; n=14) following the AZ/AZ scheme (right panel). Red bars represent geometric

475   mean values. r and P values were determined by two-tailed Spearman's correlation (**d-e, g-h, l-o**).

476   Statistical significance was determined by two-tailed Mann-Whitney test followed by Holm-Šídák

477   test for multiple comparisons (**f, j-k, p**), or by Wilcoxon matched-pairs signed rank test for paired

478   observations followed by Holm-Šídák test for multiple comparisons (**b-c, i**).

479

480

481   **Fig. S2**
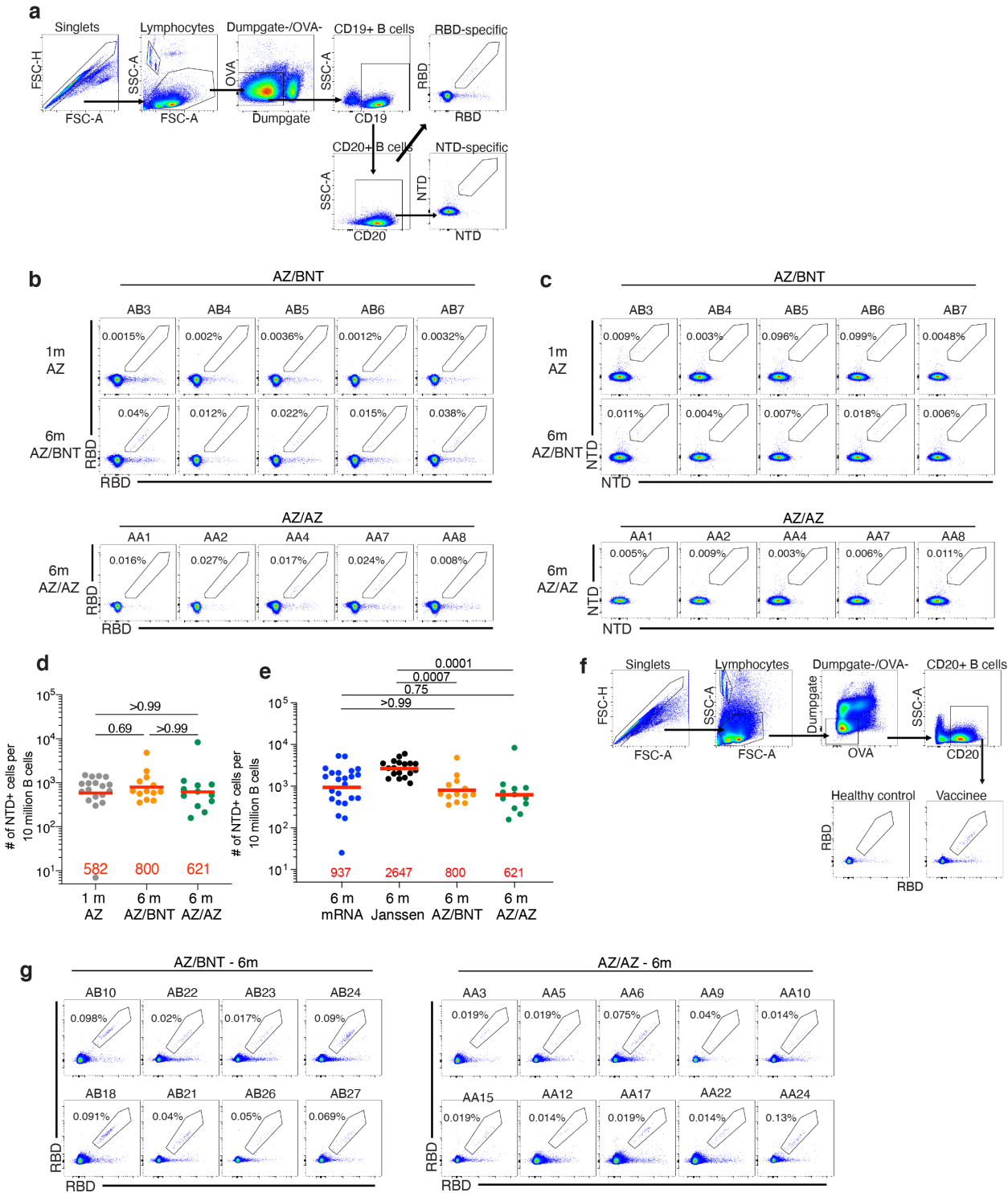
483   **Fig. S2: Flow Cytometry**. **a**, Gating strategy for phenotyping. Gating was on lymphocytes

484   singlets that were CD19+ or CD20+ and CD3-CD8-CD16-Ova-. Antigen-specific cells were

27

485   detected based on binding to Wuhan-Hu-1 RBD-PE+ and RBD-AF647+, or to Wuhan-Hu-1 NTD-

486   BrilliantViolet-711+ and NTD- BrilliantViolet-421+. Counting beads were added to each sample

487   and gated based on forward scatter (FSC) and side scatter (SSC) as per manufacturer instructions.

488   **b-c**, Representative flow cytometry plots of **b**, RBD-binding B cells or **c**, NTD-binding B cells in

489   5 individuals 1 month(m) after AZ prime and 6 months after initial dose. **d-e**, Graph showing the

490   number of NTD-BV711 and NTD-BV421 binding B cells. **f**, Gating strategy for single-cell sorting

491   for CD20+ B cells for RBD-PE and RBD-AF647. **g**, Representative flow cytometry plots showing

492   dual AlexaFluor-647- and PE-Wuhan-Hu-1-RBD binding, single-cell sorted B cells from AZ/BNT

493   and AZ/AZ vaccinees 6m after initial dose.

494

495   **Fig. S3**

496
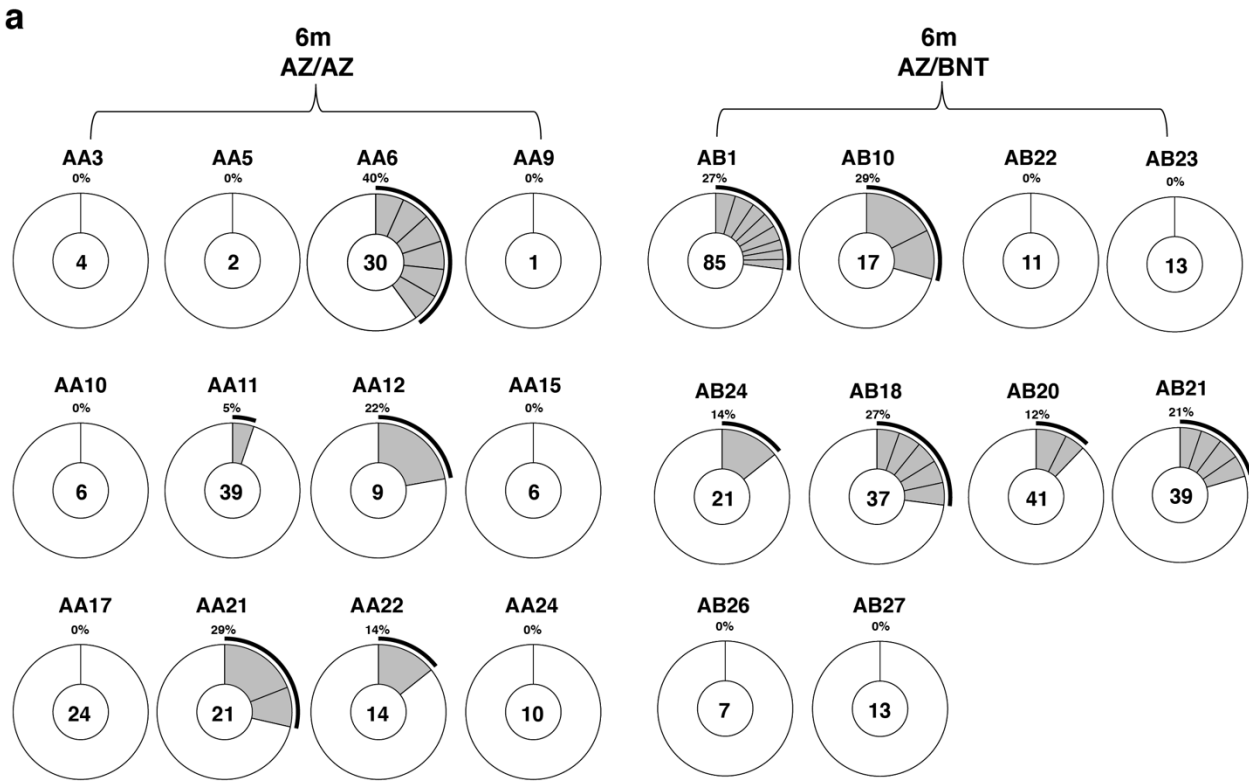
497   **Fig. S3: Clonality of anti-SARS-CoV-2 Wuhan-Hu-1 RBD antibody**

28

498   Pie charts show the distribution of IgG antibody sequences obtained from MBCs from Wuhan-

499   Hu-1 RBD-specific memory B cells of AZ/BNT and AZ/AZ vaccinees 6 m after initial dose. The

500   number inside the circle indicates the number of sequences analyzed for the individual denoted

501   above the circle.

502

503   **Fig. S4**

504
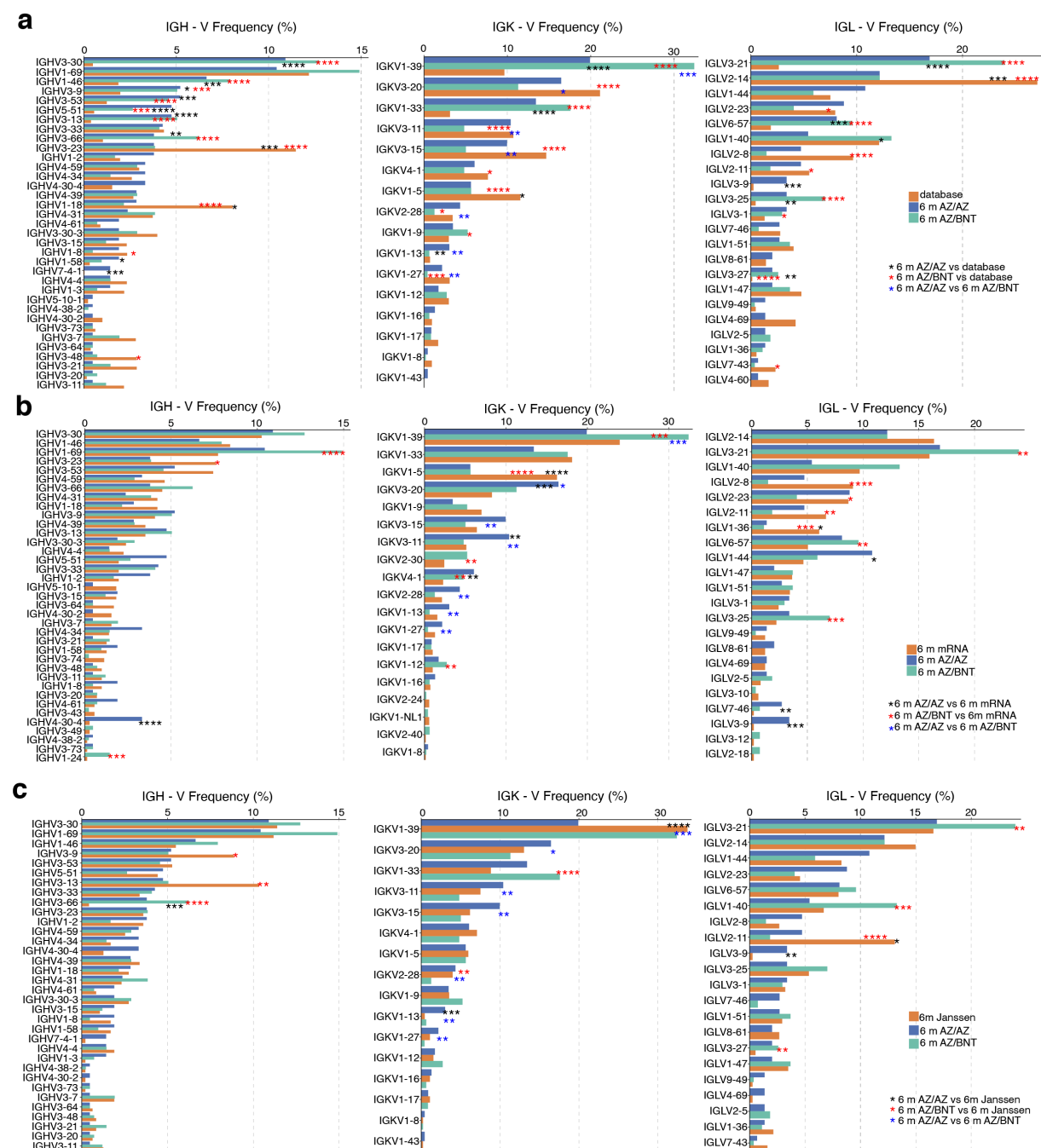
Fig. S4 Frequency distribution of human V genes. a-c Comparison of the frequency distribution

of human V genes for heavy chain and light chains of anti-RBD Wuhan-Hu-1 antibodies from this

study and from a database of shared clonotypes of human B cell receptor generated by Cinque

Soto et al (Soto et al., 2019). Graph shows relative abundance of human IGHV, IGKV and IGLV

509   genes, with 6 m AZ/AZ antibodies (blue) and AZ/BNT antibodies (green). **a,** Sequence Read

510   Archive accession SRP010970(orange); **b,** antibodies from mRNA vaccinees 6 months(m) after

511   initial dose (orange) (Cho et al., 2021); **c,** antibodies from Janssen Ad26.COV2.S vaccinees 6 m

512   after prime (orange) (Cho et al., 2022). Statistical significance was determined by two-sided

513   binomial test. * = p≤0.05, ** = p≤0.01, *** = p≤0.001, **** = p≤0.0001.

514

515   **Fig. S5**

516

517

518
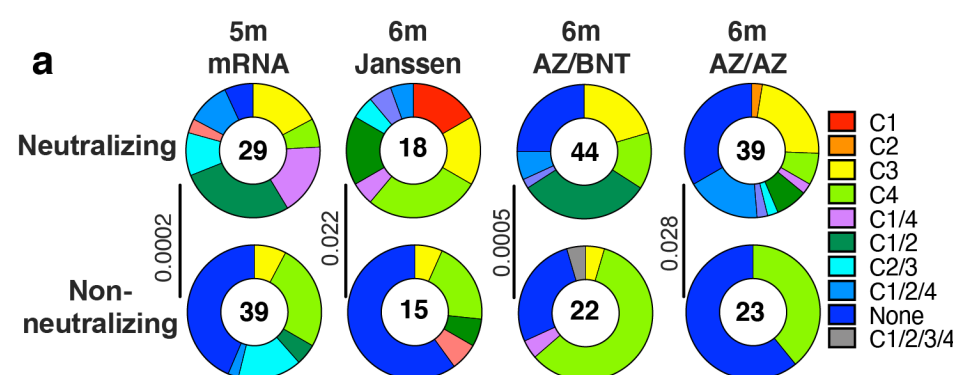
519   **Fig. S5 Epitope mapping.**

520   **a.** Results of epitope mapping performed by competition BLI. Pie charts show the distribution of

521   the antibody classes among all neutralizing antibodies against Wuhan-Hu-1 and none-neutralizing

522   antibodies obtained from mRNA vaccinees at 6 m after initial dose (n=68) (Cho et al., 2021),

523   Janssen vaccinees at 6 m (n=33) after prime (Cho et al., 2022), to mAbs cloned from AZ/AZ

524   (n=62) or AZ/BNT(n=66) vaccinees 6 m after initial dose. Pie charts were compared using a two-

525   tailed Fisher's exact test.

526

527   **Fig. S6**
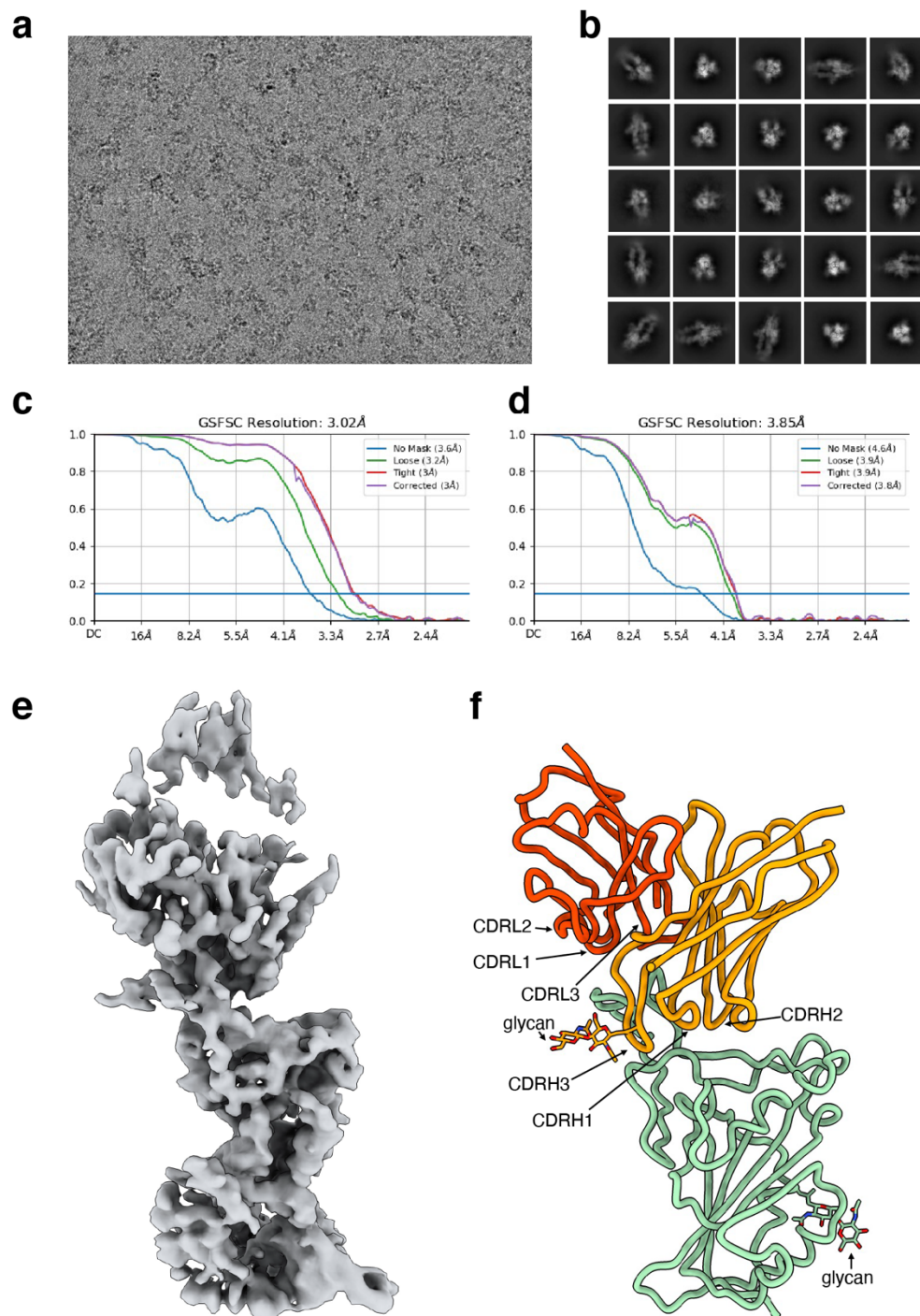
Fig. S6 Cryo-EM data processing

a, Representative cryo-EM micrograph from whole dataset. **b**, 2D class averages of selected particles for homogeneous refinement. **c**, Gold-standard Fourier shell correlation curves for the whole map of S 6P bound to AZ090 Fabs. **d**, Gold-standard Fourier shell correlation curves for the locally refined reconstruction of the RBD-AZ090 Fab region. **e**, cryo-EM density of RBD-

534   AZ090 Fab region. **f**, Model of Fab fragment bound to RBD of SARS-CoV-2 was shown by

535   cartoon. The glycans were shown by stick. The heavy chain of AZ090 was colored orange and the

536   light chain of AZ090 was colored orange red.

33

537 **Fig. S7**

a

AZ090_HC	QVQLVQSGPEVKKPGTSVKVSCKASQFTFSISAVQWVRQARGQRLEWMGWIVVGSGNTDY	60
AZ107_HC	QVQLVQSGPEVKKPGTSVRVSCKASGFTFDTSAVQWVRQARGQSLEWIGWIVVGSGNTNF	60
S2E12_HC	QVQLVQSGPEVKKPGTSVRVSCKASGFTFTSSAVQWVRQARGQRLEWVGWIVVGSGNTNY	60
A23-58.1_HC	QMQLVQSGPEVKKPGTSVKVSCKASGFTFTSSAVQWVRQARGQRLEWIGWIVVGSGNTNY	60
B1-182.1_HC	QMQLVQSGPEVKKPGTSVKVSCKASGFTFTSSAVQWVRQARGQRLEWIGWIVVGSGNTNY	60
CS44_HC	QVQLVQSGPEVKKPGTSVKVSCKASGITFTSSAVQWVRQARGQRLEWIGWIVVGSGNTNY	60
COVOX-253_HC	QVQLVQSGPEVKKPGTSVKVSCKASGFTFTTSAVQWVRQARGQRLEWIGWIVVGSGNTNY	60
COVOX-253H55L_HC	QVQLVQSGPEVKKPGTSVKVSCKASGFTFTTSAVQWVRQARGQRLEWIGWIVVGSGNTNY	60
CV07-287_HC	QVQLVQSGPEVKKPGTSVKVSCKASGFTFTSSAMQWVRQARGQRLEWIGWIVVGSGNTNY	60
	*:**************:****** :** **:********* ***:**********::	

AZ090_HC	AQRFQERVTISRDMSAGTVYMELRSLRSEDTAVYYCAAPYCNKTNCRDGFDMWGQGTMVT	120
AZ107_HC	AQKFQERVTLTRDMSTSTAYMELSSLRSEDTAVYYCAAPYCSGGTCSDGFDIWGQGTMVT	120
S2E12_HC	AQKFHERVTITRDMSTSTAYMELSSLRSEDTAVYYCASPYCSGGSCSDGFDIWGQGTMVT	120
A23-58.1_HC	AQKFQERVTITRDMSTSTAYMELSSLRSEDTAVYYCAAPNCSNVVCYDGFDIWGQGTMVT	120
B1-182.1_HC	AQKFQERVTITRDMSTSTAYMELSSLRSEDTAVYYCAAPYCSGGSCFDGFDIWGQGTMVT	120
CS44_HC	AQKFQERVTITRDMSTSTAYMELSSLRSEDTAVYYCAAPYCSGGTCHDGFDIWGQGTMVT	120
COVOX-253_HC	AQKFQERVTITRDMSTTTAYMELSSLRSEDTAVYFCAAPHCNSTSCYDAFDIWGQGTMVT	120
COVOX-253H55L_HC	AQKFQERVTITRDMSTTTAYMELSSLRSEDTAVYFCAAPHCNSTSCYDAFDIWGQGTMVT	120
CV07-287_HC	AQKFQERVTITRDMSTSTAYMELSSLRSEDTAVYYCASSTNCYDAFDIWGQGTMVT	120
	:*:**::****: *.**** **********:**:* *. * *.**:*********	

AZ090_HC	VSS	123
AZ107_HC	VSS	123
S2E12_HC	VSS	123
A23-58.1_HC	VSS	123
B1-182.1_HC	VSS	123
CS44_HC	VSS	123
COVOX-253_HC	VSS	123
COVOX-253H55L_HC	VSS	123
CV07-287_HC	VSS	123
	***	

b

Legend:
- COVOX-253H55L
- B1-182.1
- C544
- CV07-287
- A23-58.1
- S2E12
- COVOX-253
- AZ090

c

AZ090   S2E12   A23-58.1   B1-182.1

COVOX-253   COVOX-253H55L   C544   CV07-287

538

539

34

540 **Fig. S7 Comparison of AZ090 and previous resolved antibodies.**

541 **a**, Multiple sequence alignment of RBDs was processed by Clustal Omega(Sievers et al., 2011).

542 **b**, Structure of AZ090 and previous resolved antibodies encoded by same heavy chains were

543 aligned. Different Fab-RBD structures were colored respectively. **c**, Structures from **b** were

544 shown by cartoon. The RBDs were colored green, the heavy chains were colored royal blue and

545 the light chains were colored light blue. The glycans on the heavy chains were shown by stick.

546

547 **Materials and Methods**

548

549 **Study participants**.

550 Health-care workers receiving routine COVID-19 vaccination were enrolled in the EICOV and

551 COVIM prospective observational cohort studies conducted at Charité–Universitätsmedizin

552 Berlin (Berlin, Germany), after written informed consent was obtained. EICOV was approved by

553 the ethics committee of Charité–Universitätsmedizin Berlin (EA4/245/20), and COVIM was

554 approved by the Federal Institute for Vaccines and Biomedicines (Paul Ehrlich Institute) and by

555 the Ethics committee of the state of Berlin (EudraCT-2021–001512–28). Both studies were

556 conducted in accordance with the guidelines of Good Clinical Practice (ICH 1996) and the

557 Declaration of Helsinki. Health-care workers at Charité–Universitätsmedizin Berlin were offered

558 either two doses of BNT162b2 3 weeks apart or an initial dose of ChAdOx1 nCov-19 followed

559 by a heterologous boost with BNT162b2 10–12 weeks later. The vaccine regimen depended on

560 availability and current official recommendations. Health-care workers who received an initial

561 dose of ChAdOx1 nCov-19 were also free to choose a homologous booster with ChAdOx1

562 nCov-19 10–12 weeks later. (Hillus et al., 2021) For detailed participant characteristics see Table

563   S1 and previous publications (Cho et al., 2021; Cho et al., 2022; Muecksch et al., 2022). Cohort

564   sample analyses were performed under an existing Rockefeller University IRB-approved

565   protocol (DRO-1006).

566

567   **Blood samples processing and storage.**

568   Blood samples were collected in Heparin and Serum-gel monovette tubes (Greiner bio one).

569   Peripheral Blood Mononuclear Cells (PBMCs) were isolated by gradient centrifugation and

570   stored in liquid nitrogen in the presence of Fetal Calf Serum (FCS) and Dimethylsulfoxide

571   (DMSO). Heparinized plasma and serum samples were fractioned by centrifugation, aliquoted

572   and stored at -80°C until analysis. Prior to experiments, aliquots of plasma samples were heat-

573   inactivated (56°C for 30 minutes) and then stored at 4°C.

574

575   **ELISAs**

576   Enzyme-Linked Immunosorbent Assays (ELISAs) (Amanat et al., 2020; Grifoni et al., 2020) to

577   evaluate antibodies binding to SARS-CoV-2 RBD were performed by coating of high-binding

578   96-half-well plates (Corning 3690) with 50 µl per well of a 1µg/ml protein solution in Phosphate-

579   buffered Saline (PBS) overnight at 4°C. Plates were washed 6 times with washing buffer (1×

580   PBS with 0.05% Tween-20 (Sigma-Aldrich)) and incubated with 170 µl per well blocking buffer

581   (1× PBS with 2% BSA and 0.05% Tween-20 (Sigma)) for 1 hour at room temperature.

582   Immediately after blocking, monoclonal antibodies or plasma samples were added in PBS and

583   incubated for 1 hour at room temperature. Plasma samples were assayed at a 1:66 starting

584   dilution and 10 additional threefold serial dilutions. Monoclonal antibodies were tested at 10

585   µg/ml starting concentration and 10 additional fourfold serial dilutions. Plates were washed 6

36

586   times with washing buffer and then incubated with anti-human IgG, IgM or IgA secondary

587   antibody conjugated to horseradish peroxidase (HRP) (Jackson ImmunoResearch 109-036-088,

588   109-035-129, and Sigma A0295) in blocking buffer at a 1:5,000 dilution (IgM and IgG) or

589   1:3,000 dilution (IgA). Plates were developed by addition of the HRP substrate, 3,3',5,5'-

590   Tetramethylbenzidine (TMB) (ThermoFisher) for 10 minutes (plasma samples) or 4 minutes

591   (monoclonal antibodies). The developing reaction was stopped by adding 50 μl of 1 M H_2SO_4

592   and absorbance was measured at 450 nm with an ELISA microplate reader (FluoStar Omega,

593   BMG Labtech) with Omega and Omega MARS software for analysis. For plasma samples, a

594   positive control (plasma from participant COV72, diluted 66.6-fold and ten additional threefold

595   serial dilutions in PBS) was added to every assay plate for normalization. The average of its

596   signal was used for normalization of all the other values on the same plate with Excel software

597   before calculating the area under the curve using Prism V9.1 (GraphPad). Negative controls of

598   pre-pandemic plasma samples from healthy donors were used for validation (for more details,

599   please see (Robbiani et al., 2020)). For monoclonal antibodies, the ELISA half-maximal

600   concentration (EC_{50}) was determined using four-parameter nonlinear regression (GraphPad

601   Prism V9.1). EC_{50}s above 1000 ng/mL were considered non-binders.

602

603   **Proteins**

604   The mammalian expression vector encoding the Receptor Binding-Domain (RBD) of SARS-

605   CoV-2 (GenBank MN985325.1; Spike (S) protein residues 319-539) was previously described

606   (Barnes et al., 2020). Mammalian expression vector encoding the SARS-CoV-2 Wuhan-Hu-1

607   NTD (GenBank MN985325.1; S protein residues 14-307) was previously described (Wang et al.,

608   2022a).

37

609

SARS-CoV-2 pseudotyped reporter virus

A panel of plasmids expressing RBD-mutant SARS-CoV-2 spike proteins in the context of

pSARS-CoV-2-S $_{\Delta19}$ has been described (Cho et al., 2021; Muecksch et al., 2021; Wang et al.,

2021d; Weisblum et al., 2020). Variant pseudoviruses resembling SARS-CoV-2 variants Delta

(B.1.617.2) and Omicron BA.1 (B.1.1.529) have been described before (Cho et al., 2021;

Schmidt et al., 2021a; Wang et al., 2021c) and were generated by introduction of substitutions

using synthetic gene fragments (IDT) or overlap extension PCR mediated mutagenesis and

Gibson assembly. Specifically, the variant-specific deletions and substitutions introduced were:

Delta: T19R, Δ156-158, L452R, T478K, D614G, P681R, D950N

Delta-RBD: L452R, T478K

Omicron BA.1: A67V, Δ69-70, T95I, G142D, Δ143-145, Δ211, L212I, ins214EPE, G339D,

S371L, S373P, S375F, K417N, N440K, G446S, S477N, T478K, E484A, Q493K, G496S,

Q498R, N501Y, Y505H, T547K, D614G, H655Y, H679K, P681H, N764K, D796Y, N856K,

Q954H, N969H, N969K, L981F

Deletions/substitutions corresponding to variants of concern listed above, were incorporated into

a spike protein that also includes the R683G substitution, which disrupts the furin cleavage site

and increases particle infectivity. Neutralizing activity against mutant pseudoviruses were

compared to a wildtype (WT) SARS-CoV-2 spike sequence (NC_045512), carrying R683G

where appropriate.

629

SARS-CoV-2 pseudotyped particles were generated as previously described (Robbiani et al.,

2020; Schmidt et al., 2020). Briefly, 293T (CRL-11268) cells were obtained from ATCC, and

632   the cells were transfected with pNL4-3 ΔEnv-nanoluc and pSARS-CoV-2-S$_{\Delta 19}$. Particles were

633   harvested 48 hours post-transfection, filtered and stored at -80°C.

634

635   **Pseudotyped virus neutralization assay**

636   Four- to five-fold serially diluted pre-pandemic negative control plasma from healthy donors,

637   plasma from individuals who received Ad26.COV2.S vaccines, or monoclonal antibodies were

638   incubated with SARS-CoV-2 pseudotyped virus for 1 hour at 37 °C. The mixture was

639   subsequently incubated with 293T$_{Ace2}$ cells (Robbiani et al., 2020) (for all WT neutralization

640   assays) or HT1080Ace2 cl14 (for all mutant panels and variant neutralization assays) cells

641   (Wang et al., 2021d) for 48 hours after which cells were washed with PBS and lysed with

642   Luciferase Cell Culture Lysis 5× reagent (Promega). Nanoluc Luciferase activity in lysates was

643   measured using the Nano-Glo Luciferase Assay System (Promega) with the Glomax Navigator

644   (Promega) or ClarioStar Microplate Multimode Reader (BMG). The relative luminescence units

645   were normalized to those derived from cells infected with SARS-CoV-2 pseudotyped virus in the

646   absence of plasma or monoclonal antibodies. The half-maximal neutralization titers for plasma

647   (NT$_{50}$) or half-maximal and 90% inhibitory concentrations for monoclonal antibodies (IC$_{50}$ and

648   IC$_{90}$) were determined using four-parameter nonlinear regression (least squares regression

649   method without weighting; constraints: top=1, bottom=0) (GraphPad Prism).

650

651   **Biotinylation of viral protein for use in flow cytometry**

652   Purified and Avi-tagged SARS-CoV-2 Wuhan-Hu-1 RBD and NTD were biotinylated using the

653   Biotin-Protein Ligase-BIRA kit according to manufacturer's instructions (Avidity) as described

654   before (Robbiani et al., 2020). Ovalbumin (Sigma, A5503-1G) was biotinylated using the EZ-

655   Link Sulfo-NHS-LC-Biotinylation kit according to the manufacturer's instructions (Thermo

656   Scientific). Biotinylated ovalbumin was conjugated to streptavidin-BB515 (BD, 564453). RBD

657   was conjugated to streptavidin-PE (BD Biosciences, 554061) and streptavidin-AF647

658   (Biolegend, 405237) (Robbiani et al., 2020). NTD was conjugated to streptavidin-BV421

659   (Biolegend, 405225) and streptavidin-BV711 (BD Biosciences, 563262).

660

Flow cytometry and single cell sorting

662   Single-cell sorting by flow cytometry was described previously (Robbiani et al., 2020). Briefly,

663   peripheral blood mononuclear cells were enriched for B cells by negative selection using a pan-

664   B-cell isolation kit according to the manufacturer's instructions (Miltenyi Biotec, 130-101-638).

665   The enriched B cells were incubated in Flourescence-Activated Cell-sorting (FACS) buffer (1×

666   PBS, 2% FCS, 1 mM ethylenediaminetetraacetic acid (EDTA)) with the following anti-human

667   antibodies (all at 1:200 dilution): anti-CD20-PECy7 (BD Biosciences, 335793), anti-CD3-APC-

668   eFluro780 (Invitrogen, 47-0037-41), anti-CD8-APC-eFluor780 (Invitrogen, 47-0086-42), anti-

669   CD16-APC-eFluor780 (Invitrogen, 47-0168-41), anti-CD14-APC-eFluor780 (Invitrogen, 47-

670   0149-42), as well as Zombie NIR (BioLegend, 423105) and fluorophore-labeled Wuhan-Hu-1

671   RBD, NTD, and ovalbumin (Ova) for 30 min on ice. AccuCheck Counting Beads (Life

672   Technologies, PCB100) were added to each sample according to manufacturer's instructions.

673   Single CD3-CD8-CD14-CD16−CD20+Ova− B cells that were RBD-PE+RBD-AF647+ were

674   sorted into individual wells of 96-well plates containing 4 μl of lysis buffer (0.5× PBS, 10 mM

675   Dithiothreitol (DTT), 3,000 units/ml RNasin Ribonuclease Inhibitors (Promega, N2615)) per

676   well using a FACS Aria III and FACSDiva software (Becton Dickinson) for acquisition and

40

677   FlowJo for analysis. The sorted cells were frozen on dry ice, and then stored at −80 °C or

678   immediately used for subsequent RNA reverse transcription.

679

680   **Antibody sequencing, cloning and expression**

681   Antibodies were identified and sequenced as described previously (Robbiani et al., 2020; Wang

682   et al., 2021b). In brief, RNA from single cells was reverse-transcribed (SuperScript III Reverse

683   Transcriptase, Invitrogen, 18080-044) and the cDNA was stored at −20 °C or used for

684   subsequent amplification of the variable IGH, IGL and IGK genes by nested PCR and Sanger

685   sequencing. Sequence analysis was performed using MacVector. Amplicons from the first PCR

686   reaction were used as templates for sequence- and ligation-independent cloning into antibody

687   expression vectors. Recombinant monoclonal antibodies were produced and purified as

688   previously described (Robbiani et al., 2020).

689

690   **Biolayer interferometry**

691   Biolayer interferometry assays were performed as previously described (Robbiani et al., 2020).

692   Briefly, we used the Octet Red instrument (ForteBio) at 30°C with shaking at 1,000 r.p.m.

693   Epitope binding assays were performed with protein A biosensor (ForteBio 18-5010), following

694   the manufacturer's protocol "classical sandwich assay" as follows: (1) Sensor check: sensors

695   immersed 30 sec in buffer alone (buffer ForteBio 18-1105), (2) Capture 1st Ab: sensors

696   immersed 10 min with Ab1 at 10 µg/mL, (3) Baseline: sensors immersed 30 sec in buffer alone,

697   (4) Blocking: sensors immersed 5 min with IgG isotype control at 10 µg/mL. (5) Baseline:

698   sensors immersed 30 sec in buffer alone, (6) Antigen association: sensors immersed 5 min with

699   RBD at 10 µg/mL. (7) Baseline: sensors immersed 30 sec in buffer alone. (8) Association Ab2:

700   sensors immersed 5 min with Ab2 at 10 µg/mL. Affinity measurement of anti-SARS-CoV-2

701   IgGs binding were corrected by subtracting the signal obtained from traces performed with IgGs

702   in the absence of RBD. The kinetic analysis using protein A biosensor (ForteBio 18-5010) was

703   performed as follows: (1) baseline: 60sec immersion in buffer. (2) loading: 200sec immersion in

704   a solution with IgGs 10 µg/ml. (3) baseline: 200sec immersion in buffer. (4) Association: 300sec

705   immersion in solution with RBD at 20, 10, or 5 µg/ml (5) dissociation: 600sec immersion in

706   buffer. Curve fitting was performed using a fast 1:1 binding model and the Data analysis

707   software (ForteBio). Mean K_D values were determined by averaging all binding curves that

708   matched the theoretical fit with an R^2 value ≥ 0.8.Curve fitting was performed using the Fortebio

709   Octet Data analysis software (ForteBio).

710

711   **Recombinant protein expression**

712   Stabilized SARS-CoV-2 6P ectodomain and Fabs were expressed and purified as previously

713   described(Wang et al., 2022b). Briefly, constructs encoding the stabilized spike of SARS-CoV-2

714   ectodomain(Hsieh et al., 2020) were used to transiently transfect Expi293F cells (Gibco).

715   Supernatants were harvested after four days, and S 6P proteins were purified by nickel affinity

716   following with size-exclusion chromatography. Peak fractions from size-exclusion

717   chromatography were identified by native gel analysis for spike trimer fractions.

718

719   **Cryo-EM sample preparation**

720   Purified Fabs were mixed with S 6P protein at a 1.1:1 M ratio of Fab-to-protomer for 30 min at

721   room temperature. Fab-S complexes were deposited on a freshly glow-discharged 400 mesh,

722   1.2/1.3 Quantifoil grid (Electron Microscopy Sciences). Immediately prior to deposition of 3 mL

723   of complex onto grid, fluorinated octyl-maltoside (Anatrace) was added to the sample to a final

724   concentration of 0.02% w/v. Samples were vitrified in 100% liquid ethane using a Mark IV

725   Vitrobot (Thermo Fisher) after blotting at 22 C° and 100% humidity for 3s with filter paper.

726

727   **Cryo-EM data collection and processing**

728   Single-particle cryo-EM data were collected on a Titan Krios transmission electron microscope

729   (Thermo Fisher) equipped with a Gatan K3 direct detector, operating at 300 kV and controlled

730   using SerialEM automated data collection software (Mastronarde, 2005). A total dose of 56.56

731   e/Å^2 was accumulated on each movie with a pixel size of 0.515 and a defocus range of -0.8 and

732   2.0 µm. Movie frame alignment, CTF estimation, particle-picking and extraction were carried

733   out using cryoSPARC v3.3.1(Punjani et al., 2017). Reference-free particle picking and extraction

734   were performed on dose-weighted micrographs. A subset of 4x-downsampled particles were

735   used to conduct several rounds of reference-free 2D classification, then the selected Fab-S

736   particles were extracted, 2x-downsampled, yielding a pixel size of 1.03 Å. The particles were

737   used to generate *ab initio* models, which were then used for heterogeneous refinement of the

738   entire dataset in cryoSPARC. Particles belonging to classes that resembled Fab-S structures were

739   homogeneous refined following with non-uniform refinement until imported into Relion 3.1.3

740   for CTF refinement. The particles were then imported into cryoSPARC for heterogenerous

741   refinement. Particles belonging to classes with better Fab density were selected and subjected to

742   another round of homogeneous refinement following with non-uniform refinement. To improve

743   the density of the RBD/AZ090interface, several rounds of local refinement were then performed

744   using different soft masks. Reported resolutions are based on the gold-standard Fourier shell

745   correlation of 0.143 criterion (Bell et al., 2016).

746

Cryo-EM structure modeling and analysis

748   UCSF Chimera(Pettersen et al., 2004) and Coot(Emsley et al., 2010) were used to fit atomic

749   models into the locally refined cryoEM map. Models were refined and validated by

750   Phenix(Liebschner et al., 2019). Figures were generated using UCSF ChimeraX(Goddard et al.,

751   2018).

752

Computational analyses of antibody sequences

754   Antibody sequences were trimmed based on quality and annotated using Igblastn v.1.14. with

755   IMGT domain delineation system. Annotation was performed systematically using Change-O

756   toolkit v.0.4.540 (Gupta et al., 2015). Clonality of heavy and light chain was determined using

757   DefineClones.py implemented by Change-O v0.4.5 (Gupta et al., 2015). The script calculates the

758   Hamming distance between each sequence in the data set and its nearest neighbor. Distances are

759   subsequently normalized and to account for differences in junction sequence length, and

760   clonality is determined based on a cut-off threshold of 0.15. Heavy and light chains derived from

761   the same cell were subsequently paired, and clonotypes were assigned based on their V and J

762   genes using in-house R and Perl scripts. All scripts and the data used to process antibody

763   sequences are publicly available on GitHub

764   (https://github.com/stratust/igpipeline/tree/igpipeline2_timepoint_v2).

765   The frequency distributions of human V genes in anti-SARS-CoV-2 antibodies from this study

766   was compared to 131,284,220 IgH and IgL sequences generated by (Soto et al., 2019) and

767   downloaded from cAb-Rep (Guo et al., 2019), a database of human shared BCR clonotypes

768   available at https://cab-rep.c2b2.columbia.edu/. Based on the 150 distinct V genes that make up

44

769   the 1099 analyzed sequences from Ig repertoire of the 6 participants present in this study, we

770   selected the IgH and IgL sequences from the database that are partially coded by the same V

771   genes and counted them according to the constant region. The frequencies shown in Fig. S4 are

772   relative to the source and isotype analyzed. We used the two-sided binomial test to check

773   whether the number of sequences belonging to a specific *IGHV* or *IGLV* gene in the repertoire is

774   different according to the frequency of the same IgV gene in the database. Adjusted p-values

775   were calculated using the false discovery rate (FDR) correction. Significant differences are

776   denoted with stars.

777

778   Nucleotide somatic hypermutation and Complementarity-Determining Region 3 (CDR3) length

779   were determined using in-house R and Perl scripts. For somatic hypermutations (SHM), *IGHV*

780   and *IGLV* nucleotide sequences were aligned against their closest germlines using Igblastn and

781   the number of differences were considered nucleotide mutations. The average number of

782   mutations for V genes was calculated by dividing the sum of all nucleotide mutations across all

783   participants by the number of sequences used for the analysis.

784

785   **Data presentation**

786   Figures arranged in Adobe Illustrator 2022.

787

788   **Data availability statement:** Data are provided in Tables S1-5. The raw sequencing data and

789   computer scripts associated with Fig. 2 have been deposited at Github

790   (https://github.com/stratust/igpipeline/tree/igpipeline2_timepoint_v2). This study also uses data

791   from (DeWitt et al., 2016), cAb-Rep (https://cab-rep.c2b2.columbia.edu/)(Guo et al., 2019),

792   Sequence Read Archive (accession SRP010970), and from (Soto et al., 2019).

793

794   **Code availability statement:** Computer code to process the antibody sequences is available at

795   GitHub (https://github.com/stratust/igpipeline/tree/igpipeline2_timepoint_v2).

796

821

822   **Author information:** Z.W., F.Muecksch, F.Muenn and A.C. contributed equally to this work.

823
824   **Author Contributions:** Z.W., F.M., A.C., T.H., P.D.B., M.C.N. and C.G. conceived, designed,

825   and analyzed the experiments. F.K., L.S., M. C. and C.G. designed clinical protocols. F.M. Z.W.,

826   A.C., S.H., R.R., T.B.T, J.D., E.B., C.G.-C., K.Y., and C.G. carried out experiments. B.J. and

827   A.G., produced antibodies. A.G. produced SARS-CoV-2 proteins. F.Muenn, P.T.-L., D.H., F.K.,

828   L.S., M.T., K.G.M., I.S., C.G and M.C. recruited participants, executed clinical protocols, and

829   processed samples. T.Y.O. and V.R. performed bioinformatic analysis. Z.W., M.C.N. and C.G.

830   wrote the manuscript with input from all co-authors.

831

832   **Corresponding authors:** Correspondence should be addressed to Michel C. Nussenzweig or

833   Christian Gaebler

834

838

839

References

Amanat, F., D. Stadlbauer, S. Strohmeier, T.H.O. Nguyen, V. Chromikova, M. McMahon, K. Jiang, G.A. Arunkumar, D. Jurczyszak, J. Polanco, M. Bermudez-Gonzalez, G. Kleiner, T. Aydillo, L. Miorin, D.S. Fierer, L.A. Lugo, E.M. Kojic, J. Stoever, S.T.H. Liu, C. Cunningham-Rundles, P.L. Felgner, T. Moran, A. Garcia-Sastre, D. Caplivski, A.C. Cheng, K. Kedzierska, O. Vapalahti, J.M. Hepojoki, V. Simon, and F. Krammer. 2020. A serological assay to detect SARS-CoV-2 seroconversion in humans. *Nat Med* 26:1033-1036.

Amanna, I.J., N.E. Carlson, and M.K. Slifka. 2007. Duration of humoral immunity to common viral and vaccine antigens. *N Engl J Med* 357:1903-1915.

Andrews, N., E. Tessier, J. Stowe, C. Gower, F. Kirsebom, R. Simmons, E. Gallagher, S. Thelwall, N. Groves, G. Dabrera, R. Myers, C.N.J. Campbell, G. Amirthalingam, M. Edmunds, M. Zambon, K. Brown, S. Hopkins, M. Chand, S.N. Ladhani, M. Ramsay, and J. Lopez Bernal. 2022. Duration of Protection against Mild and Severe Disease by Covid-19 Vaccines. *N Engl J Med* 386:340-350.

Barnes, C.O., C.A. Jette, M.E. Abernathy, K.A. Dam, S.R. Esswein, H.B. Gristick, A.G. Malyutin, N.G. Sharaf, K.E. Huey-Tubman, Y.E. Lee, D.F. Robbiani, M.C. Nussenzweig, A.P. West, Jr., and P.J. Bjorkman. 2020. SARS-CoV-2 neutralizing antibody structures inform therapeutic strategies. *Nature* 588:682-687.

Barros-Martins, J., S.I. Hammerschmidt, A. Cossmann, I. Odak, M.V. Stankov, G. Morillas Ramos, A. Dopfer-Jablonka, A. Heidemann, C. Ritter, M. Friedrichsen, C. Schultze-Florey, I. Ravens, S. Willenzon, A. Bubke, J. Ristenpart, A. Janssen, G. Ssebyatika, G. Bernhardt, J. Munch, M. Hoffmann, S. Pohlmann, T. Krey, B. Bosnjak, R. Forster, and G.M.N. Behrens. 2021. Immune responses against SARS-CoV-2 variants after heterologous and homologous ChAdOx1 nCoV-19/BNT162b2 vaccination. *Nat Med* 27:1525-1529.

Bednarski, E., P.M.D. Rio Estrada, J. DaSilva, C. Boukadida, F. Zhang, Y.A. Luna-Villalobos, X. Rodríguez-Rangel, E. Pitén-Isidro, E. Luna-García, D.D. Rivera, D.M. López-Sánchez, D. Tapia-Trejo, M. Soto-Nava, M. Astorga-Castañeda, J.O. Martínez-Moreno, G.S. Urbina-Granados, J.A. Jiménez-Jacinto, F.J. Serna Alvarado, Y.E. Enriquez-López, O. López-Arellano, G. Reyes-Teran, P.D. Bieniasz, S. Avila-Rios, and T. Hatziioannou. 2022. Antibody and memory B-cell immunity in a heterogeneously SARS-CoV-2 infected and vaccinated population. *medRxiv*

Bell, J.M., M. Chen, P.R. Baldwin, and S.J. Ludtke. 2016. High resolution single particle refinement in EMAN2.1. *Methods* 100:25-34.

Bergwerk, M., T. Gonen, Y. Lustig, S. Amit, M. Lipsitch, C. Cohen, M. Mandelboim, E.G. Levin, C. Rubin, V. Indenbaum, I. Tal, M. Zavitan, N. Zuckerman, A. Bar-Chaim, Y. Kreiss, and G. Regev-Yochay. 2021. Covid-19 Breakthrough Infections in Vaccinated Health Care Workers. *N Engl J Med* 385:1474-1484.

Botton, J., L. Semenzato, M.J. Jabagi, B. Baricault, A. Weill, R. Dray-Spira, and M. Zureik. 2022. Effectiveness of Ad26.COV2.S Vaccine vs BNT162b2 Vaccine for COVID-19 Hospitalizations. *JAMA Netw Open* 5:e220868.

Braeye, T., L. Catteau, R. Brondeel, J.A.F. van Loenhout, K. Proesmans, L. Cornelissen, H. Van Oyen, V. Stouten, P. Hubin, M. Billuart, A. Djiena, R. Mahieu, N. Hammami, D. Van Cauteren, and C. Wyndham-Thomas. 2022. Vaccine effectiveness against onward

885   transmission of SARS-CoV2-infection by variant of concern and time since vaccination,
886   Belgian contact tracing, 2021. *Vaccine* 40:3027-3037.
887   Cho, A., F. Muecksch, D. Schaefer-Babajew, Z. Wang, S. Finkin, C. Gaebler, V. Ramos, M.
888   Cipolla, P. Mendoza, M. Agudelo, E. Bednarski, J. DaSilva, I. Shimeliovich, J. Dizon, M.
889   Daga, K.G. Millard, M. Turroja, F. Schmidt, F. Zhang, T.B. Tanfous, M. Jankovic, T.Y.
890   Oliveria, A. Gazumyan, M. Caskey, P.D. Bieniasz, T. Hatziioannou, and M.C.
891   Nussenzweig. 2021. Anti-SARS-CoV-2 receptor-binding domain antibody evolution
892   after mRNA vaccination. *Nature* 600:517-522.
893   Cho, A., F. Muecksch, Z. Wang, T.B. Tanfous, J. DaSilva, R. Raspe, B. Johnson, E. Bednarski,
894   V. Ramos, D. Schaefer-Babajew, I. Shimeliovich, J. Dizon, K.-H. Yao, F. Schmidt, K.G.
895   Millard, M. Turroja, M. Jankovic, T.Y. Oliveira, A. Gazumyan, C. Gaebler, M. Caskey,
896   T. Hatziioannou, P.D. Bieniasz, and M.C. Nussenzweig. 2022. Antibody evolution to
897   SARS-CoV-2 after single-dose Ad26.COV2.S vaccine. *bioRxiv* 2022.2003.2031.486548.
898   Dejnirattisai, W., D. Zhou, H.M. Ginn, H.M.E. Duyvesteyn, P. Supasa, J.B. Case, Y. Zhao, T.S.
899   Walter, A.J. Mentzer, C. Liu, B. Wang, G.C. Paesen, J. Slon-Campos, C. Lopez-
900   Camacho, N.M. Kafai, A.L. Bailey, R.E. Chen, B. Ying, C. Thompson, J. Bolton, A.
901   Fyfe, S. Gupta, T.K. Tan, J. Gilbert-Jaramillo, W. James, M. Knight, M.W. Carroll, D.
902   Skelly, C. Dold, Y. Peng, R. Levin, T. Dong, A.J. Pollard, J.C. Knight, P. Klenerman, N.
903   Temperton, D.R. Hall, M.A. Williams, N.G. Paterson, F.K.R. Bertram, C.A. Siebert,
904   D.K. Clare, A. Howe, J. Radecke, Y. Song, A.R. Townsend, K.A. Huang, E.E. Fry, J.
905   Mongkolsapaya, M.S. Diamond, J. Ren, D.I. Stuart, and G.R. Screaton. 2021. The
906   antigenic anatomy of SARS-CoV-2 receptor binding domain. *Cell* 184:2183-2200 e2122.
907   DeWitt, W.S., P. Lindau, T.M. Snyder, A.M. Sherwood, M. Vignali, C.S. Carlson, P.D.
908   Greenberg, N. Duerkopp, R.O. Emerson, and H.S. Robins. 2016. A Public Database of
909   Memory and Naive B-Cell Receptor Sequences. *PLoS One* 11:e0160853.
910   Emsley, P., B. Lohkamp, W.G. Scott, and K. Cowtan. 2010. Features and development of Coot.
911   *Acta Crystallogr D Biol Crystallogr* 66:486-501.
912   Feng, S., D.J. Phillips, T. White, H. Sayal, P.K. Aley, S. Bibi, C. Dold, M. Fuskova, S.C. Gilbert,
913   I. Hirsch, H.E. Humphries, B. Jepson, E.J. Kelly, E. Plested, K. Shoemaker, K.M.
914   Thomas, J. Vekemans, T.L. Villafana, T. Lambe, A.J. Pollard, M. Voysey, and C.V.T.G.
915   Oxford. 2021. Correlates of protection against symptomatic and asymptomatic SARS-
916   CoV-2 infection. *Nat Med* 27:2032-2040.
917   Gaebler, C., Z. Wang, J.C.C. Lorenzi, F. Muecksch, S. Finkin, M. Tokuyama, A. Cho, M.
918   Jankovic, D. Schaefer-Babajew, T.Y. Oliveira, M. Cipolla, C. Viant, C.O. Barnes, Y.
919   Bram, G. Breton, T. Hagglof, P. Mendoza, A. Hurley, M. Turroja, K. Gordon, K.G.
920   Millard, V. Ramos, F. Schmidt, Y. Weisblum, D. Jha, M. Tankelevich, G. Martinez-
921   Delgado, J. Yee, R. Patel, J. Dizon, C. Unson-O'Brien, I. Shimeliovich, D.F. Robbiani, Z.
922   Zhao, A. Gazumyan, R.E. Schwartz, T. Hatziioannou, P.J. Bjorkman, S. Mehandru, P.D.
923   Bieniasz, M. Caskey, and M.C. Nussenzweig. 2021. Evolution of antibody immunity to
924   SARS-CoV-2. *Nature* 591:639-644.
925   Goddard, T.D., C.C. Huang, E.C. Meng, E.F. Pettersen, G.S. Couch, J.H. Morris, and T.E.
926   Ferrin. 2018. UCSF ChimeraX: Meeting modern challenges in visualization and analysis.
927   *Protein Sci* 27:14-25.
928   Grifoni, A., D. Weiskopf, S.I. Ramirez, J. Mateus, J.M. Dan, C.R. Moderbacher, S.A. Rawlings,
929   A. Sutherland, L. Premkumar, R.S. Jadi, D. Marrama, A.M. de Silva, A. Frazier, A.F.
930   Carlin, J.A. Greenbaum, B. Peters, F. Krammer, D.M. Smith, S. Crotty, and A. Sette.

931   2020. Targets of T Cell Responses to SARS-CoV-2 Coronavirus in Humans with
932   COVID-19 Disease and Unexposed Individuals. *Cell* 181:1489-1501 e1415.

933 Guo, Y., K. Chen, P.D. Kwong, L. Shapiro, and Z. Sheng. 2019. cAb-Rep: A Database of
934   Curated Antibody Repertoires for Exploring Antibody Diversity and Predicting Antibody
935   Prevalence. *Front Immunol* 10:2365.

936 Gupta, N.T., J.A. Vander Heiden, M. Uduman, D. Gadala-Maria, G. Yaari, and S.H. Kleinstein.
937   2015. Change-O: a toolkit for analyzing large-scale B cell immunoglobulin repertoire
938   sequencing data. *Bioinformatics* 31:3356-3358.

939 Hall, V.G., V.H. Ferreira, H. Wood, M. Ierullo, B. Majchrzak-Kita, K. Manguiat, A. Robinson,
940   V. Kulasingam, A. Humar, and D. Kumar. 2022. Delayed-interval BNT162b2 mRNA
941   COVID-19 vaccination enhances humoral immunity and induces robust T cell responses.
942   *Nature Immunology* 23:380-385.

943 Hillus, D., T. Schwarz, P. Tober-Lau, K. Vanshylla, H. Hastor, C. Thibeault, S. Jentzsch, E.T.
944   Helbig, L.J. Lippert, P. Tscheak, M.L. Schmidt, J. Riege, A. Solarek, C. von Kalle, C.
945   Dang-Heine, H. Gruell, P. Kopankiewicz, N. Suttorp, C. Drosten, H. Bias, J. Seybold,
946   E.C.S. Group, F. Klein, F. Kurth, V.M. Corman, and L.E. Sander. 2021. Safety,
947   reactogenicity, and immunogenicity of homologous and heterologous prime-boost
948   immunisation with ChAdOx1 nCoV-19 and BNT162b2: a prospective cohort study.
949   *Lancet Respir Med* 9:1255-1265.

950 Hsieh, C.L., J.A. Goldsmith, J.M. Schaub, A.M. DiVenere, H.C. Kuo, K. Javanmardi, K.C. Le,
951   D. Wrapp, A.G. Lee, Y. Liu, C.W. Chou, P.O. Byrne, C.K. Hjorth, N.V. Johnson, J.
952   Ludes-Meyers, A.W. Nguyen, J. Park, N. Wang, D. Amengor, J.J. Lavinder, G.C.
953   Ippolito, J.A. Maynard, I.J. Finkelstein, and J.S. McLellan. 2020. Structure-based design
954   of prefusion-stabilized SARS-CoV-2 spikes. *Science* 369:1501-1505.

955 Kaku, C.I., E.R. Champney, J. Normark, M. Garcia, C.E. Johnson, C. Ahlm, W. Christ, M.
956   Sakharkar, M.E. Ackerman, J. Klingstrom, M.N.E. Forsell, and L.M. Walker. 2022.
957   Broad anti-SARS-CoV-2 antibody immunity induced by heterologous ChAdOx1/mRNA-
958   1273 vaccination. *Science* 375:1041-1047.

959 Khoury, D.S., D. Cromer, A. Reynaldi, T.E. Schlub, A.K. Wheatley, J.A. Juno, K. Subbarao, S.J.
960   Kent, J.A. Triccas, and M.P. Davenport. 2021. Neutralizing antibody levels are highly
961   predictive of immune protection from symptomatic SARS-CoV-2 infection. *Nat Med*
962   27:1205-1211.

963 Klok, F.A., M. Pai, M.V. Huisman, and M. Makris. 2022. Vaccine-induced immune thrombotic
964   thrombocytopenia. *Lancet Haematol* 9:e73-e80.

965 Li, D., G.D. Sempowski, K.O. Saunders, P. Acharya, and B.F. Haynes. 2022. SARS-CoV-2
966   Neutralizing Antibodies for COVID-19 Prevention and Treatment. *Annu Rev Med* 73:1-
967   16.

968 Liebschner, D., P.V. Afonine, M.L. Baker, G. Bunkoczi, V.B. Chen, T.I. Croll, B. Hintze, L.W.
969   Hung, S. Jain, A.J. McCoy, N.W. Moriarty, R.D. Oeffner, B.K. Poon, M.G. Prisant, R.J.
970   Read, J.S. Richardson, D.C. Richardson, M.D. Sammito, O.V. Sobolev, D.H. Stockwell,
971   T.C. Terwilliger, A.G. Urzhumtsev, L.L. Videau, C.J. Williams, and P.D. Adams. 2019.
972   Macromolecular structure determination using X-rays, neutrons and electrons: recent
973   developments in Phenix. *Acta Crystallogr D Struct Biol* 75:861-877.

974 Lin, D.Y., Y. Gu, B. Wheeler, H. Young, S. Holloway, S.K. Sunny, Z. Moore, and D. Zeng.
975   2022. Effectiveness of Covid-19 Vaccines over a 9-Month Period in North Carolina. *N
976   Engl J Med* 386:933-941.

977   Mallapaty, S., E. Callaway, M. Kozlov, H. Ledford, J. Pickrell, and R. Van Noorden. 2021. How
978   COVID vaccines shaped 2021 in eight powerful charts. *Nature* 600:580-583.
979   Mathieu, E., H. Ritchie, E. Ortiz-Ospina, M. Roser, J. Hasell, C. Appel, C. Giattino, and L.
980   Rodes-Guirao. 2021. A global database of COVID-19 vaccinations. *Nat Hum Behav*
981   5:947-953.
982   Mesin, L., A. Schiepers, J. Ersching, A. Barbulescu, C.B. Cavazzoni, A. Angelini, T. Okada, T.
983   Kurosaki, and G.D. Victora. 2020. Restricted Clonality and Limited Germinal Center
984   Reentry Characterize Memory B Cell Reactivation by Boosting. *Cell* 180:92-106 e111.
985   Muecksch, F., Z. Wang, A. Cho, C. Gaebler, T. Ben Tanfous, J. DaSilva, E. Bednarski, V.
986   Ramos, S. Zong, B. Johnson, R. Raspe, D. Schaefer-Babajew, I. Shimeliovich, M. Daga,
987   K.H. Yao, F. Schmidt, K.G. Millard, M. Turroja, M. Jankovic, T.Y. Oliveira, A.
988   Gazumyan, M. Caskey, T. Hatziioannou, P.D. Bieniasz, and M.C. Nussenzweig. 2022.
989   Increased Memory B Cell Potency and Breadth After a SARS-CoV-2 mRNA Boost.
990   *Nature*
991   Muecksch, F., Y. Weisblum, C.O. Barnes, F. Schmidt, D. Schaefer-Babajew, Z. Wang, C.L. JC,
992   A.I. Flyak, A.T. DeLaitsch, K.E. Huey-Tubman, S. Hou, C.A. Schiffer, C. Gaebler, J. Da
993   Silva, D. Poston, S. Finkin, A. Cho, M. Cipolla, T.Y. Oliveira, K.G. Millard, V. Ramos,
994   A. Gazumyan, M. Rutkowska, M. Caskey, M.C. Nussenzweig, P.J. Bjorkman, T.
995   Hatziioannou, and P.D. Bieniasz. 2021. Affinity maturation of SARS-CoV-2 neutralizing
996   antibodies confers potency, breadth, and resilience to viral escape mutations. *Immunity*
997   54:1853-1868 e1857.
998   Nordstrom, P., M. Ballin, and A. Nordstrom. 2021. Effectiveness of heterologous ChAdOx1
999   nCoV-19 and mRNA prime-boost vaccination against symptomatic Covid-19 infection in
1000   Sweden: A nationwide cohort study. *Lancet Reg Health Eur* 11:100249.
1001   Normark, J., L. Vikstrom, Y.D. Gwon, I.L. Persson, A. Edin, T. Bjorsell, A. Dernstedt, W.
1002   Christ, S. Tevell, M. Evander, J. Klingstrom, C. Ahlm, and M. Forsell. 2021.
1003   Heterologous ChAdOx1 nCoV-19 and mRNA-1273 Vaccination. *N Engl J Med*
1004   385:1049-1051.
1005   Pettersen, E.F., T.D. Goddard, C.C. Huang, G.S. Couch, D.M. Greenblatt, E.C. Meng, and T.E.
1006   Ferrin. 2004. UCSF Chimera--a visualization system for exploratory research and
1007   analysis. *J Comput Chem* 25:1605-1612.
1008   Pozzetto, B., V. Legros, S. Djebali, V. Barateau, N. Guibert, M. Villard, L. Peyrot, O. Allatif,
1009   J.B. Fassier, A. Massardier-Pilonchery, K. Brengel-Pesce, M. Yaugel-Novoa, S. Denolly,
1010   B. Boson, T. Bourlet, A. Bal, M. Valette, T. Andrieu, B. Lina, g. Covid-Ser study, F.L.
1011   Cosset, S. Paul, T. Defrance, J. Marvel, T. Walzer, and S. Trouillet-Assant. 2021.
1012   Immunogenicity and efficacy of heterologous ChAdOx1-BNT162b2 vaccination. *Nature*
1013   600:701-706.
1014   Punjani, A., J.L. Rubinstein, D.J. Fleet, and M.A. Brubaker. 2017. cryoSPARC: algorithms for
1015   rapid unsupervised cryo-EM structure determination. *Nat Methods* 14:290-296.
1016   Reincke, S.M., M. Yuan, H.C. Kornau, V.M. Corman, S. van Hoof, E. Sanchez-Sendin, M.
1017   Ramberger, W. Yu, Y. Hua, H. Tien, M.L. Schmidt, T. Schwarz, L.M. Jeworowski, S.E.
1018   Brandl, H.F. Rasmussen, M.A. Homeyer, L. Stoffler, M. Barner, D. Kunkel, S. Huo, J.
1019   Horler, N. von Wardenburg, I. Kroidl, T.M. Eser, A. Wieser, C. Geldmacher, M.
1020   Hoelscher, H. Ganzer, G. Weiss, D. Schmitz, C. Drosten, H. Pruss, I.A. Wilson, and J.
1021   Kreye. 2022. SARS-CoV-2 Beta variant infection elicits potent lineage-specific and
1022   cross-reactive antibodies. *Science* 375:782-787.

1023 Robbiani, D.F., C. Gaebler, F. Muecksch, J.C.C. Lorenzi, Z. Wang, A. Cho, M. Agudelo, C.O.
1024   Barnes, A. Gazumyan, S. Finkin, T. Hagglof, T.Y. Oliveira, C. Viant, A. Hurley, H.H.
1025   Hoffmann, K.G. Millard, R.G. Kost, M. Cipolla, K. Gordon, F. Bianchini, S.T. Chen, V.
1026   Ramos, R. Patel, J. Dizon, I. Shimeliovich, P. Mendoza, H. Hartweger, L. Nogueira, M.
1027   Pack, J. Horowitz, F. Schmidt, Y. Weisblum, E. Michailidis, A.W. Ashbrook, E. Waltari,
1028   J.E. Pak, K.E. Huey-Tubman, N. Koranda, P.R. Hoffman, A.P. West, Jr., C.M. Rice, T.
1029   Hatziioannou, P.J. Bjorkman, P.D. Bieniasz, M. Caskey, and M.C. Nussenzweig. 2020.
1030   Convergent antibody responses to SARS-CoV-2 in convalescent individuals. *Nature*
1031   584:437-442.
1032 Schmidt, F., F. Muecksch, Y. Weisblum, J. Da Silva, E. Bednarski, A. Cho, Z. Wang, C.
1033   Gaebler, M. Caskey, M.C. Nussenzweig, T. Hatziioannou, and P.D. Bieniasz. 2021a.
1034   Plasma Neutralization of the SARS-CoV-2 Omicron Variant. *N Engl J Med*
1035 Schmidt, F., Y. Weisblum, F. Muecksch, H.H. Hoffmann, E. Michailidis, J.C.C. Lorenzi, P.
1036   Mendoza, M. Rutkowska, E. Bednarski, C. Gaebler, M. Agudelo, A. Cho, Z. Wang, A.
1037   Gazumyan, M. Cipolla, M. Caskey, D.F. Robbiani, M.C. Nussenzweig, C.M. Rice, T.
1038   Hatziioannou, and P.D. Bieniasz. 2020. Measuring SARS-CoV-2 neutralizing antibody
1039   activity using pseudotyped and chimeric viruses. *J Exp Med* 217:
1040 Schmidt, T., V. Klemis, D. Schub, J. Mihm, F. Hielscher, S. Marx, A. Abu-Omar, L. Ziegler, C.
1041   Guckelmus, R. Urschel, S. Schneitler, S.L. Becker, B.C. Gartner, U. Sester, and M.
1042   Sester. 2021b. Immunogenicity and reactogenicity of heterologous ChAdOx1 nCoV-
1043   19/mRNA vaccination. *Nat Med* 27:1530-1535.
1044 Self, W.H., M.W. Tenforde, J.P. Rhoads, M. Gaglani, A.A. Ginde, D.J. Douin, S.M. Olson, H.K.
1045   Talbot, J.D. Casey, N.M. Mohr, A. Zepeski, T. McNeal, S. Ghamande, K.W. Gibbs, D.C.
1046   Files, D.N. Hager, A. Shehu, M.E. Prekker, H.L. Erickson, M.N. Gong, A. Mohamed,
1047   D.J. Henning, J.S. Steingrub, I.D. Peltan, S.M. Brown, E.T. Martin, A.S. Monto, A.
1048   Khan, C.L. Hough, L.W. Busse, C.C. Ten Lohuis, A. Duggal, J.G. Wilson, A.J. Gordon,
1049   N. Qadir, S.Y. Chang, C. Mallow, C. Rivas, H.M. Babcock, J.H. Kwon, M.C. Exline, N.
1050   Halasa, J.D. Chappell, A.S. Lauring, C.G. Grijalva, T.W. Rice, I.D. Jones, W.B.
1051   Stubblefield, A. Baughman, K.N. Womack, C.J. Lindsell, K.W. Hart, Y. Zhu, L. Mills,
1052   S.N. Lester, M.M. Stumpf, E.A. Naioti, M. Kobayashi, J.R. Verani, N.J. Thornburg,
1053   M.M. Patel, and I.V.Y. Network. 2021. Comparative Effectiveness of Moderna, Pfizer-
1054   BioNTech, and Janssen (Johnson & Johnson) Vaccines in Preventing COVID-19
1055   Hospitalizations Among Adults Without Immunocompromising Conditions - United
1056   States, March-August 2021. *MMWR Morb Mortal Wkly Rep* 70:1337-1343.
1057 Sievers, F., A. Wilm, D. Dineen, T.J. Gibson, K. Karplus, W. Li, R. Lopez, H. McWilliam, M.
1058   Remmert, J. Soding, J.D. Thompson, and D.G. Higgins. 2011. Fast, scalable generation
1059   of high-quality protein multiple sequence alignments using Clustal Omega. *Mol Syst Biol*
1060   7:539.
1061 Soto, C., R.G. Bombardi, A. Branchizio, N. Kose, P. Matta, A.M. Sevy, R.S. Sinkovits, P.
1062   Gilchuk, J.A. Finn, and J.E. Crowe, Jr. 2019. High frequency of shared clonotypes in
1063   human B cell receptor repertoires. *Nature* 566:398-402.
1064 Tortorici, M.A., M. Beltramello, F.A. Lempp, D. Pinto, H.V. Dang, L.E. Rosen, M. McCallum,
1065   J. Bowen, A. Minola, S. Jaconi, F. Zatta, A. De Marco, B. Guarino, S. Bianchi, E.J.
1066   Lauron, H. Tucker, J. Zhou, A. Peter, C. Havenar-Daughton, J.A. Wojcechowskyj, J.B.
1067   Case, R.E. Chen, H. Kaiser, M. Montiel-Ruiz, M. Meury, N. Czudnochowski, R.
1068   Spreafico, J. Dillen, C. Ng, N. Sprugasci, K. Culap, F. Benigni, R. Abdelnabi, S.C. Foo,

52

1069   M.A. Schmid, E. Cameroni, A. Riva, A. Gabrieli, M. Galli, M.S. Pizzuto, J. Neyts, M.S.
1070   Diamond, H.W. Virgin, G. Snell, D. Corti, K. Fink, and D. Veesler. 2020. Ultrapotent
1071   human antibodies protect against SARS-CoV-2 challenge via multiple mechanisms.
1072   *Science* 370:950-957.
1073 Tortorici, M.A., and D. Veesler. 2019. Chapter Four - Structural insights into coronavirus entry.
1074   In Advances in Virus Research. F.A. Rey, editor Academic Press, 93-116.
1075 Vilches, T.N., S.M. Moghadas, P. Sah, M.C. Fitzpatrick, A. Shoukat, A. Pandey, and A.P.
1076   Galvani. 2022. Estimating COVID-19 Infections, Hospitalizations, and Deaths Following
1077   the US Vaccination Campaigns During the Pandemic. *JAMA Netw Open* 5:e2142725.
1078 Voysey, M., S.A. Costa Clemens, S.A. Madhi, L.Y. Weckx, P.M. Folegatti, P.K. Aley, B.
1079   Angus, V.L. Baillie, S.L. Barnabas, Q.E. Bhorat, S. Bibi, C. Briner, P. Cicconi, E.A.
1080   Clutterbuck, A.M. Collins, C.L. Cutland, T.C. Darton, K. Dheda, C. Dold, C.J.A.
1081   Duncan, K.R.W. Emary, K.J. Ewer, A. Flaxman, L. Fairlie, S.N. Faust, S. Feng, D.M.
1082   Ferreira, A. Finn, E. Galiza, A.L. Goodman, C.M. Green, C.A. Green, M. Greenland, C.
1083   Hill, H.C. Hill, I. Hirsch, A. Izu, D. Jenkin, C.C.D. Joe, S. Kerridge, A. Koen, G. Kwatra,
1084   R. Lazarus, V. Libri, P.J. Lillie, N.G. Marchevsky, R.P. Marshall, A.V.A. Mendes, E.P.
1085   Milan, A.M. Minassian, A. McGregor, Y.F. Mujadidi, A. Nana, S.D. Padayachee, D.J.
1086   Phillips, A. Pittella, E. Plested, K.M. Pollock, M.N. Ramasamy, A.J. Ritchie, H.
1087   Robinson, A.V. Schwarzbold, A. Smith, R. Song, M.D. Snape, E. Sprinz, R.K.
1088   Sutherland, E.C. Thomson, M.E. Török, M. Toshner, D.P.J. Turner, J. Vekemans, T.L.
1089   Villafana, T. White, C.J. Williams, A.D. Douglas, A.V.S. Hill, T. Lambe, S.C. Gilbert,
1090   A.J. Pollard, M. Aban, K.W.M. Abeyskera, J. Aboagye, M. Adam, K. Adams, J.P.
1091   Adamson, G. Adewatan, S. Adlou, K. Ahmed, Y. Akhalwaya, S. Akhalwaya, A. Alcock,
1092   A. Ali, E.R. Allen, L. Allen, F.B. Alvernaz, F.S. Amorim, C.S. Andrade, F. Andritsou, R.
1093   Anslow, E.H. Arbe-Barnes, M.P. Ariaans, B. Arns, L. Arruda, L. Assad, P.D.A. Azi,
1094   L.D.A. Azi, G. Babbage, C. Bailey, K.F. Baker, M. Baker, N. Baker, P. Baker, I.
1095   Baleanu, D. Bandeira, A. Bara, M.A.S. Barbosa, D. Barker, G.D. Barlow, E. Barnes, A.S.
1096   Barr, J.R. Barrett, J. Barrett, K. Barrett, L. Bates, A. Batten, K. Beadon, E. Beales, R.
1097   Beckley, S. Belij-Rammerstorfer, J. Bell, D. Bellamy, S. Belton, A. Berg, L. Bermejo, E.
1098   Berrie, L. Berry, D. Berzenyi, A. Beveridge, K.R. Bewley, I. Bharaj, S. Bhikha, A.E.
1099   Bhorat, Z.E. Bhorat, E.M. Bijker, S. Birch, G. Birch, K. Birchall, A. Bird, O. Bird, K.
1100   Bisnauthsing, M. Bittaye, L. Blackwell, R. Blacow, H. Bletchly, C.L. Blundell, S.R.
1101   Blundell, P. Bodalia, E. Bolam, E. Boland, D. Bormans, N. Borthwick, F. Bowring, A.
1102   Boyd, P. Bradley, T. Brenner, A. Bridges-Webb, P. Brown, C. Brown, C. Brown-
1103   O'Sullivan, S. Bruce, E. Brunt, W. Budd, Y.A. Bulbulia, M. Bull, J. Burbage, A. Burn,
1104   K.R. Buttigieg, N. Byard, I. Cabrera Puig, A. Calvert, S. Camara, M. Cao, F. Cappuccini,
1105   R. Cardona, J.R. Cardoso, M. Carr, M.W. Carroll, A. Carson-Stevens, Y.d.M. Carvalho,
1106   H.R. Casey, P. Cashen, T.R.Y. Castro, L.C. Castro, K. Cathie, A. Cavey, J. Cerbino-
1107   Neto, L.F.F. Cezar, J. Chadwick, C. Chanice, D. Chapman, S. Charlton, K.S. Cheliotis, I.
1108   Chelysheva, O. Chester, E. Chiplin, S. Chita, J.-S. Cho, L. Cifuentes, E. Clark, M. Clark,
1109   R. Colin-Jones, S.L.K. Collins, H. Colton, C.P. Conlon, S. Connarty, N. Coombes, C.
1110   Cooper, R. Cooper, L. Cornelissen, T. Corrah, C.A. Cosgrove, F.B. Costa, T. Cox,
1111   W.E.M. Crocker, S. Crosbie, D. Cullen, D.R.M.F. Cunha, C.J. Cunningham, F.C.
1112   Cuthbertson, D.M. da Costa, S.N.F. Da Guarda, L.P. da Silva, A.C. da Silva Moraes, B.E.
1113   Damratoski, Z. Danos, M.T.D.C. Dantas, M.S. Datoo, C. Datta, M. Davids, S.L. Davies,
1114   K. Davies, H. Davies, S. Davies, J. Davies, E.J. Davis, J. Davis, J.A.M. de Carvalho, J.

1115   De Jager, S. de Jesus Jnr, L.M. De Oliveira Kalid, D. Dearlove, T. Demissie, A. Desai, S.
1116   Di Marco, C. Di Maso, T. Dinesh, C. Docksey, T. Dong, F.R. Donnellan, T.G. Dos
1117   Santos, T.G. Dos Santos, E.P. Dos Santos, N. Douglas, C. Downing, J. Drake, R. Drake-
1118   Brockman, R. Drury, J. Du Plessis, S.J. Dunachie, A. Duncan, N.J.W. Easom, M.
1119   Edwards, N.J. Edwards, F. Edwards, O.M. El Muhanna, S.C. Elias, B. Ellison-Handley,
1120   M.J. Elmore, M.R. English, A. Esmail, Y.M. Essack, M. Farooq, S. Fedosyuk, S. Felle,
1121   S. Ferguson, C. Ferreira Da Silva, S. Field, R. Fisher, J. Fletcher, H. Fofie, H. Fok, K.J.
1122   Ford, R. Fothergill, J. Fowler, P.H.A. Fraiman, E. Francis, M.M. Franco, J. Frater,
1123   M.S.M. Freire, S.H. Fry, S. Fudge, R. Furlan Filho, J. Furze, M. Fuskova, P. Galian-
1124   Rubio, H. Garlant, M. Gavrila, K.A. Gibbons, C. Gilbride, H. Gill, K. Godwin, K.
1125   Gokani, M.L.F. Gonçalves, I.G.S. Gonzalez, J. Goodall, J. Goodwin, A. Goondiwala, K.
1126   Gordon-Quayle, G. Gorini, A. Goyanna, J. Grab, L. Gracie, J. Green, N. Greenwood, J.
1127   Greffrath, M.M. Groenewald, A. Gunawardene, G. Gupta, M. Hackett, B. Hallis, M.
1128   Hamaluba, E. Hamilton, J. Hamlyn, D. Hammersley, A.T. Hanrath, B. Hanumunthadu,
1129   S.A. Harris, C. Harris, T.D. Harrison, D. Harrison, T.A. Harris-Wright, T.C. Hart, B.
1130   Hartnell, J. Haughney, S. Hawkins, L.Y.M. Hayano, I. Head, P.T. Heath, J.A. Henry, M.
1131   Hermosin Herrera, D.B. Hettle, C. Higa, J. Hill, G. Hodges, S. Hodgson, E. Horne, M.M.
1132   Hou, C.F. Houlihan, E. Howe, N. Howell, J. Humphreys, H.E. Humphries, K. Hurley, C.
1133   Huson, C. Hyams, A. Hyder-Wright, S. Ikram, A. Ishwarbhai, P. Iveson, V. Iyer, F.
1134   Jackson, S. Jackson, S. Jaumdally, H. Jeffers, N. Jesudason, C. Jones, C. Jones, K. Jones,
1135   E. Jones, M.R. Jorge, A. Joshi, E.A.M.S. Júnior, R. Kailath, F. Kana, A. Kar, K.
1136   Karampatsas, M. Kasanyinga, L. Kay, J. Keen, J. Kellett Wright, E.J. Kelly, D. Kelly,
1137   D.M. Kelly, S. Kelly, D. Kerr, L. Khan, B. Khozoee, A. Khurana, S. Kidd, A. Killen, J.
1138   Kinch, P. Kinch, L.D.W. King, T.B. King, L. Kingham, P. Klenerman, D.M. Kluczna, F.
1139   Knapper, J.C. Knight, D. Knott, S. Koleva, P.M. Lages, M. Lang, G. Lang, C.W.
1140   Larkworthy, J.P.J. Larwood, R. Law, A.M. Lawrie, E.M. Lazarus, A. Leach, E.A. Lees,
1141   A. Lelliott, N.-M. Lemm, A.E.R. Lessa, S. Leung, Y. Li, A.M. Lias, K. Liatsikos, A.
1142   Linder, S. Lipworth, S. Liu, X. Liu, A. Lloyd, S. Lloyd, L. Loew, R. Lopez Ramon, L.B.
1143   Lora, K.G. Luz, J.C. MacDonald, G. MacGregor, M. Madhavan, D.O. Mainwaring, E.
1144   Makambwa, R. Makinson, M. Malahleha, R. Malamatsho, G. Mallett, N. Manning, K.
1145   Mansatta, T. Maoko, S. Marinou, E. Marlow, G.N. Marques, P. Marriott, R.P. Marshall,
1146   J.L. Marshall, M. Masenya, M. Masilela, S.K. Masters, M. Mathew, H. Matlebjane, K.
1147   Matshidiso, O. Mazur, A. Mazzella, H. McCaughan, J. McEwan, J. McGlashan, L.
1148   McInroy, N. McRobert, S. McSwiggan, C. Megson, S. Mehdipour, W. Meijs, R.N.Õ.
1149   Mendonça, A.J. Mentzer, A.C.F. Mesquita, P. Miralhes, N. Mirtorabi, C. Mitton, S.
1150   Mnyakeni, F. Moghaddas, K. Molapo, M. Moloi, M. Moore, M. Moran, E. Morey, R.
1151   Morgans, S.J. Morris, S. Morris, H. Morrison, F. Morselli, G. Morshead, R. Morter, L.
1152   Mottay, A. Moultrie, N. Moyo, M. Mpelembue, S. Msomi, Y. Mugodi, E.
1153   Mukhopadhyay, J. Muller, A. Munro, S. Murphy, P. Mweu, C. Myerscough, G. Naik, K.
1154   Naker, E. Nastouli, B. Ndlovu, E. Nikolaou, C. Njenga, H.C. Noal, A. Noé, G. Novaes,
1155   F.L. Nugent, G.L.A. Nunes, K. O'Brien, D. O'Connor, S. Oelofse, B. Oguti, V.
1156   Olchawski, N.J. Oldfield, M.G. Oliveira, C. Oliveira, I.S.Q. Oliveira, A. Oommen-Jose,
1157   A. Oosthuizen, P. O'Reilly, P.J. O'Reilly, P. Osborne, D.R.J. Owen, L. Owen, D. Owens,
1158   N. Owino, M. Pacurar, B.V.B. Paiva, E.M.F. Palhares, S. Palmer, H.M.R.T. Parracho, K.
1159   Parsons, D. Patel, B. Patel, F. Patel, M. Patrick-Smith, R.O. Payne, Y. Peng, E.J. Penn,
1160   A. Pennington, M.P. Peralta Alvarez, B.P. Pereira Stuchi, A.L. Perez, T. Perinpanathan,

J. Perring, R. Perumal, S.Y. Petkar, T. Philip, J. Phillips, M.K. Phohu, L. Pickup, S. Pieterse, J.M. Pinheiro, J. Piper, D. Pipini, M. Plank, S. Plant, S. Pollard, J. Pooley, A. Pooran, I. Poulton, C. Powers, F.B. Presa, D.A. Price, V. Price, M.R. Primeira, P.C. Proud, S. Provstgaard-Morys, S. Pueschel, D. Pulido, S. Quaid, R. Rabara, K. Radia, D. Rajapaska, T. Rajeswaran, L. Ramos, A.S.F. Ramos, F. Ramos Lopez, T. Rampling, J. Rand, H. Ratcliffe, T. Rawlinson, D. Rea, B. Rees, M. Resuello-Dauti, E. Reyes Pabon, S. Rhead, T. Riaz, M. Ricamara, A. Richards, A. Richter, N. Ritchie, A.J. Ritchie, A.J. Robbins, H. Roberts, R.E. Robinson, S. Roche, C. Rollier, L. Rose, A.L. Ross Russell, L. Rossouw, S. Royal, I. Rudiansyah, K. Ryalls, C. Sabine, S. Saich, J.C. Sale, A.M. Salman, N. Salvador, S. Salvador, M.D. Sampaio, A.D. Samson, A. Sanchez-Gonzalez, H. Sanders, K. Sanders, E. Santos, M.F.S. Santos Guerra, I. Satti, J.E. Saunders, C. Saunders, A.B.A. Sayed, I. Schim van der Loeff, A.B. Schmid, E. Schofield, G.R. Screaton, S. Seddiqi, R.R. Segireddy, R. Senger, S. Serrano, I. Shaik, H.R. Sharpe, K. Sharrocks, R. Shaw, A. Shea, E. Sheehan, A. Shepherd, F. Shiham, S.E. Silk, L. Silva-Reyes, L.B.T.D. Silveira, M.B.V. Silveira, N. Singh, J. Sinha, D.T. Skelly, D.C. Smith, N. Smith, H.E. Smith, D.J. Smith, C.C. Smith, A.S. Soares, C. Solórzano, G.L. Sorio, K. Sorley, T. Sosa-Rodriguez, C.M.C.D.L. Souza, B.S.D.F. Souza, A.R. Souza, T. Souza Lopez, L. Sowole, A.J. Spencer, L. Spoors, L. Stafford, I. Stamford, R. Stein, L. Stockdale, L.V. Stockwell, L.H. Strickland, A. Stuart, A. Sturdy, N. Sutton, A. Szigeti, A. Tahiri-Alaoui, R. Tanner, C. Taoushanis, A.W. Tarr, R. Tarrant, K. Taylor, U. Taylor, I.J. Taylor, J. Taylor, R. te Water Naude, K. Templeton, Y. Themistocleous, A. Themistocleous, M. Thomas, K. Thomas, T.M. Thomas, A. Thombrayil, J. Thompson, F. Thompson, A. Thompson, A. Thompson, K. Thompson, V. Thornton-Jones, L.H.S. Thotusi, P.J. Tighe, L.A. Tinoco, G.F. Tiongson, B. Tladinyane, M. Tomasicchio, A. Tomic, S. Tonks, J. Towner, N. Tran, J.A. Tree, G. Trillana, C. Trinham, R. Trivett, A. Truby, B.L. Tsheko, P. Tubb, A. Turabi, R. Turner, C. Turner, N. Turner, B. Tyagi, M. Ulaszewska, B.R. Underwood, S. van Eck, R. Varughese, D. Verbart, M.K. Verheul, I. Vichos, T.A. Vieira, G. Walker, L. Walker, M.E. Wand, T. Wardell, G.M. Warimwe, S.C. Warren, B. Watkins, M.E.E. Watson, E. Watson, S. Webb, A. Webster, J. Welch, Z. Wellbelove, J.H. Wells, A.J. West, B. White, C. White, R. White, P. Williams, R.L. Williams, S. Willingham, R. Winslow, D. Woods, M. Woodyer, A.T. Worth, D. Wright, M. Wroblewska, A. Yao, Y.T.N. Yim, M.B. Zambrano, R.L. Zimmer, D. Zizi, and P. Zuidewind. 2021. Single-dose administration and the influence of the timing of the booster dose on immunogenicity and efficacy of ChAdOx1 nCoV-19 (AZD1222) vaccine: a pooled analysis of four randomised trials. *The Lancet* 397:881-891.

Wang, L., T. Zhou, Y. Zhang, E.S. Yang, C.A. Schramm, W. Shi, A. Pegu, O.K. Oloniniyi, A.R. Henry, S. Darko, S.R. Narpala, C. Hatcher, D.R. Martinez, Y. Tsybovsky, E. Phung, O.M. Abiona, A. Antia, E.M. Cale, L.A. Chang, M. Choe, K.S. Corbett, R.L. Davis, A.T. DiPiazza, I.J. Gordon, S.H. Hait, T. Hermanus, P. Kgagudi, F. Laboune, K. Leung, T. Liu, R.D. Mason, A.F. Nazzari, L. Novik, S. O'Connell, S. O'Dell, A.S. Olia, S.D. Schmidt, T. Stephens, C.D. Stringham, C.A. Talana, I.T. Teng, D.A. Wagner, A.T. Widge, B. Zhang, M. Roederer, J.E. Ledgerwood, T.J. Ruckwardt, M.R. Gaudinski, P.L. Moore, N.A. Doria-Rose, R.S. Baric, B.S. Graham, A.B. McDermott, D.C. Douek, P.D. Kwong, J.R. Mascola, N.J. Sullivan, and J. Misasi. 2021a. Ultrapotent antibodies against diverse and highly transmissible SARS-CoV-2 variants. *Science* 373:

1206 Wang, Z., J.C.C. Lorenzi, F. Muecksch, S. Finkin, C. Viant, C. Gaebler, M. Cipolla, H.H.
1207   Hoffmann, T.Y. Oliveira, D.A. Oren, V. Ramos, L. Nogueira, E. Michailidis, D.F.
1208   Robbiani, A. Gazumyan, C.M. Rice, T. Hatziioannou, P.D. Bieniasz, M. Caskey, and
1209   M.C. Nussenzweig. 2021b. Enhanced SARS-CoV-2 neutralization by dimeric IgA. *Sci*
1210   *Transl Med* 13:
1211 Wang, Z., F. Muecksch, A. Cho, C. Gaebler, H.-H. Hoffmann, V. Ramos, S. Zong, M. Cipolla,
1212   B. Johnson, F. Schmidt, J. DaSilva, E. Bednarski, T.B. Tanfous, R. Raspe, K. Yao, Y.E.
1213   Lee, T. Chen, M. Turroja, K.G. Milard, J. Dizon, A. Kaczynska, A. Gazumyan, T.Y.
1214   Oliveira, C.M. Rice, M. Caskey, P.D. Bieniasz, T. Hatziioannou, C.O. Barnes, and M.C.
1215   Nussenzweig. 2022a. Conserved Neutralizing Epitopes on the N-Terminal Domain of
1216   Variant SARS-CoV-2 Spike Proteins. *bioRxiv* 2022.2002.2001.478695.
1217 Wang, Z., F. Muecksch, A. Cho, C. Gaebler, H.H. Hoffmann, V. Ramos, S. Zong, M. Cipolla, B.
1218   Johnson, F. Schmidt, J. DaSilva, E. Bednarski, T. Ben Tanfous, R. Raspe, K. Yao, Y.E.
1219   Lee, T. Chen, M. Turroja, K.G. Milard, J. Dizon, A. Kaczynska, A. Gazumyan, T.Y.
1220   Oliveira, C.M. Rice, M. Caskey, P.D. Bieniasz, T. Hatziioannou, C.O. Barnes, and M.C.
1221   Nussenzweig. 2022b. Analysis of memory B cells identifies conserved neutralizing
1222   epitopes on the N-terminal domain of variant SARS-Cov-2 spike proteins. *Immunity*
1223 Wang, Z., F. Muecksch, D. Schaefer-Babajew, S. Finkin, C. Viant, C. Gaebler, H.H. Hoffmann,
1224   C.O. Barnes, M. Cipolla, V. Ramos, T.Y. Oliveira, A. Cho, F. Schmidt, J. da Silva, E.
1225   Bednarski, L. Aguado, J. Yee, M. Daga, M. Turroja, K.G. Millard, M. Jankovic, A.
1226   Gazumyan, Z. Zhao, C.M. Rice, P.D. Bieniasz, M. Caskey, T. Hatziioannou, and M.C.
1227   Nussenzweig. 2021c. Naturally enhanced neutralizing breadth against SARS-CoV-2 one
1228   year after infection. *Nature*
1229 Wang, Z., F. Schmidt, Y. Weisblum, F. Muecksch, C.O. Barnes, S. Finkin, D. Schaefer-
1230   Babajew, M. Cipolla, C. Gaebler, J.A. Lieberman, T.Y. Oliveira, Z. Yang, M.E.
1231   Abernathy, K.E. Huey-Tubman, A. Hurley, M. Turroja, K.A. West, K. Gordon, K.G.
1232   Millard, V. Ramos, J. Da Silva, J. Xu, R.A. Colbert, R. Patel, J. Dizon, C. Unson-
1233   O'Brien, I. Shimeliovich, A. Gazumyan, M. Caskey, P.J. Bjorkman, R. Casellas, T.
1234   Hatziioannou, P.D. Bieniasz, and M.C. Nussenzweig. 2021d. mRNA vaccine-elicited
1235   antibodies to SARS-CoV-2 and circulating variants. *Nature* 592:616-622.
1236 Watanabe, Y., L. Mendonca, E.R. Allen, A. Howe, M. Lee, J.D. Allen, H. Chawla, D. Pulido, F.
1237   Donnellan, H. Davies, M. Ulaszewska, S. Belij-Rammerstorfer, S. Morris, A.S. Krebs,
1238   W. Dejnirattisai, J. Mongkolsapaya, P. Supasa, G.R. Screaton, C.M. Green, T. Lambe, P.
1239   Zhang, S.C. Gilbert, and M. Crispin. 2021. Native-like SARS-CoV-2 Spike Glycoprotein
1240   Expressed by ChAdOx1 nCoV-19/AZD1222 Vaccine. *ACS Cent Sci* 7:594-602.
1241 Weisblum, Y., F. Schmidt, F. Zhang, J. DaSilva, D. Poston, J.C. Lorenzi, F. Muecksch, M.
1242   Rutkowska, H.H. Hoffmann, E. Michailidis, C. Gaebler, M. Agudelo, A. Cho, Z. Wang,
1243   A. Gazumyan, M. Cipolla, L. Luchsinger, C.D. Hillyer, M. Caskey, D.F. Robbiani, C.M.
1244   Rice, M.C. Nussenzweig, T. Hatziioannou, and P.D. Bieniasz. 2020. Escape from
1245   neutralizing antibodies by SARS-CoV-2 spike protein variants. *Elife* 9:
1246 Wu, F., S. Zhao, B. Yu, Y.M. Chen, W. Wang, Z.G. Song, Y. Hu, Z.W. Tao, J.H. Tian, Y.Y. Pei,
1247   M.L. Yuan, Y.L. Zhang, F.H. Dai, Y. Liu, Q.M. Wang, J.J. Zheng, L. Xu, E.C. Holmes,
1248   and Y.Z. Zhang. 2020. A new coronavirus associated with human respiratory disease in
1249   China. *Nature* 579:265-269.

1250   Yuan, M., H. Liu, N.C. Wu, C.D. Lee, X. Zhu, F. Zhao, D. Huang, W. Yu, Y. Hua, H. Tien, T.F.
1251   Rogers, E. Landais, D. Sok, J.G. Jardine, D.R. Burton, and I.A. Wilson. 2020. Structural
1252   basis of a shared antibody response to SARS-CoV-2. *Science* 369:1119-1123.
1253   Zhang, Z., J. Mateus, C.H. Coelho, J.M. Dan, C.R. Moderbacher, R.I. Galvez, F.H. Cortes, A.
1254   Grifoni, A. Tarke, J. Chang, E.A. Escarrega, C. Kim, B. Goodwin, N.I. Bloom, A.
1255   Frazier, D. Weiskopf, A. Sette, and S. Crotty. 2022. Humoral and cellular immune
1256   memory to four COVID-19 vaccines. *bioRxiv* 2022.2003.2018.484953.
1257

1258